

1 **Latest Jurassic–Early Cretaceous synrift evolution of the Torrelapaja Subbasin**
2 **(Camerós Basin): implications for Northeast Iberia palaeogeography**

3 Aurell, M. (1); Bádenas, B. (1); Castanera, D. (2); Gasca, J.M. (1); Canudo, J.I. (1); Laita, E. (1); Liesa, C.L.
4 (3)

5 *(1) Grupo Araragosaurus-IUCA, Departamento de Ciencias de la Tierra. Universidad de Zaragoza, 50009 Zaragoza, Spain*

6 *(2) Institut Català de Paleontologia Miquel Crusafont, Universitat Autònoma de Barcelona, c/Escola Industrial 23, 08201,*
7 *Sabadell, Barcelona, Spain*

8 *(3) Grupo Geotransfer, IUCA, Departamento de Ciencias de la Tierra. Universidad de Zaragoza, 50009 Zaragoza, Spain*

9
10
11 **ABSTRACT**

12 The reconstruction of the latest Jurassic–Early Cretaceous evolution of the Torrelapaja Subbasin
13 (Camerós Basin, Spain) resulted in the characterization of three synrift sequences (SS-1, SS-2 and SS-3)
14 bounded by major unconformities. Three major NW-SE normal faults combined with smaller scale faults
15 of variable direction (around NE-SW) controlled the sedimentation. The complex geometry of the
16 Torrelapaja Subbasin indicates a main extension direction of NE-SW, and a secondary NW-SE extension.
17 Sedimentation of the Tithonian–middle Berriasian SS-1 occurred in alluvial fan systems, grading upwards
18 to carbonate palustrine-lacustrine environments. A new vertebrate site with large size sauropod bones
19 has been found in the middle part of SS-1. The lower boundary of the uppermost Hauterivian–lower
20 Barremian SS-2 is locally a palaeokarst, with sedimentary infill including three new fossil sites with
21 remains of ornithopod, sauropod and theropod dinosaurs. Sedimentation of SS-2 encompasses distal
22 alluvial terrigenous facies with local palaeosoils and palustrine-lacustrine limestones grading upwards to
23 middle-distal alluvial facies. After a late Barremian–early Albian stratigraphic gap, sedimentation

24 resumed in coastal flat environments represented by the mudstones with intercalated skeletal (oyster-
25 rich) sandy limestones with carbonaceous plant remains of the SS-3. A middle-late Albian age assignment
26 of SS-3 based on regional correlation is supported by strontium isotopic data. This unit marks the first
27 Early Cretaceous marine incursion in the area from the northern Atlantic realm. This is a notable change
28 of the previous palaeogeographical reconstructions which established that the first marine
29 encroachment occurred in the early Aptian and was sourced from Tethysian domains.

30 **Key words:** *Lower Cretaceous, continental sedimentation, extensional tectonics, dinosaurs,*
31 *palaeogeography, Northeast Iberia*

32

33 1. INTRODUCTION

34 Extensional tectonics in the Iberian Basin rift system (Northeast Spain) around the Jurassic-Cretaceous
35 transition involved a major palaeogeographic change, from the setting of wide shallow-marine Jurassic
36 carbonate platforms, to continental-coastal sedimentation confined to locally subsident basins,
37 subbasins and troughs. The recorded uppermost Jurassic–Lower Cretaceous synrift deposits consist of
38 successive units separated by unconformities, the number and age of which vary from one sedimentary
39 domain to another (e.g., Salas et al., 2001; Mas et al., 2004; Liesa et al., 2019; Aurell et al., 2019b).

40 The Torrelapaja Subbasin is a relatively small (8x14 km) uppermost Jurassic–Lower Cretaceous subsident
41 area located in the southeastern edge of the Cameros Basin (Mas et al., 2002), in an area found relatively
42 close to the Maestrazgo Basin (Fig. 1A). The critical location of this subbasin between the two main
43 sedimentary domains of the latest Jurassic–Early Cretaceous Iberian Basin rift system makes its analysis
44 relevant to decipher the sedimentary evolution linked to the active extensional tectonics and to
45 understand the palaeogeography of Northeast Iberia during the latest Jurassic–Early Cretaceous. Initial
46 palaeogeographical reconstructions of Northeast Iberia considered that there was no marine connection

47 between the northern Cameros and the southern Maestrazgo sedimentary domains during the Early
48 Cretaceous (e.g., Canérot, 1974; García, 1982). However, the presence of coastal marine deposits
49 recorded in the upper part of the synrift succession in the Torrelapaja Subbasin was tentatively related
50 to an early Aptian transgressive event sourced from the southern Tethysian realm (Alonso and Mas,
51 1988, 1993). Based on this assumption, subsequent early Aptian palaeogeographical reconstructions of
52 Northeast Iberia (e.g., Salas et al., 2001; Mas et al., 2004; Suarez-González et al., 2013) proposed a
53 marine connection between the Cameros and Maestrazgo sedimentary domains through a narrow NW-
54 SE trending seaway located in the central part of the Iberian rift system. However, the data and
55 interpretation reported in our work does not support this Aptian marine connection.

56 Another point of interest of the uppermost Jurassic–Lower Cretaceous synrift successions of the Iberian
57 Basin rift system is the abundant presence of dinosaur fossil sites. The Cameros Basin has an important
58 record of dinosaur ichnites, especially in the provinces of Soria and La Rioja (e.g., Hernández-Medrano et
59 al., 2005; Moratalla and Hernán, 2010; Pérez-Lorente, 2015). Dinosaur fossil bones are known but in less
60 abundance (e.g., Canudo et al., 2010, Fuentes-Vidarte et al., 2016; Isasmendi et al., 2020). Within the
61 osteological record of Cameros, the Barremian–Aptian in the western domain (Burgos province) stands
62 out by its richness and high number of dinosaur type localities (e.g., Torcida Fernández et al., 2017).
63 Towards the east, the dinosaur fossil record is scarcer. In particular, dinosaur fossil occurrences
64 described so far in the Torrelapaja Subbasin are local and fragmentary (Royo-Torres et al., 2012; Rey-
65 Martínez and Royo-Torres, 2014). However, the data reported here show that this subbasin offers great
66 possibilities of a new significant vertebrate fossil record.

67 The main aim of this work is to characterize the latest Jurassic–Early Cretaceous tectono-sedimentary
68 evolution of the Torrelapaja Subbasin. Previous work on the area provided relevant structural,
69 stratigraphic and micropaleontological data (Schudack, 1987; Alonso and Mas, 1988, 1990; Martín-
70 Closas, 1989; Guimerà et al., 2004; Sacristán-Horcajada et al., 2011, 2012), but there is a lack of a
71 comprehensive and systematic study of the recorded sedimentary synrift successions. Accordingly, the

72 objectives of this work are: (1) to reconstruct the structure of the area, with the identification of
73 different sets of normal faults that controlled the tectono-sedimentary evolution; (2) to provide an
74 updated stratigraphic and sedimentological framework of the uppermost Jurassic–Lower Cretaceous
75 synrift successions, in order to reconstruct the depositional setting and its sedimentary evolution; (3) to
76 precise the age and palaeoenvironment of the new dinosaur fossil sites found in the course of our field
77 work, and those previously reported; (4) to discuss on the impact of the obtained results to a better
78 understanding of the palaeogeographic evolution of Northeast Iberia. Data and interpretations provided
79 here can be relevant for future tectono-sedimentary and paleontological research both on the studied
80 subbasin and nearby basins of Northeast Iberia.

81

82 **2. GEOLOGICAL SETTING**

83 The Torrelapaja Subbasin is defined here to include the Bigornia and Bijuesca troughs identified in
84 previous works (Mas et al., 2002; Guimerà et al., 2004; Sacristán-Horcajada et al., 2011, 2012). This
85 subbasin is located in the southeastern edge of the Cameros Basin (Fig. 1A), a large extensional basin
86 bounded by the so-called North and South Cameros faults. The Cameros Basin records an up to 8 km-
87 thick uppermost Jurassic–Lower Cretaceous dominant continental successions in its depocentral areas
88 (e.g. Mas et al. 2004, 2019; Guimerà et al., 2004; Casas et al., 2009; Clemente, 2010). The Torrelapaja
89 Subbasin is located between the South Cameros Fault and the Carabantes Fault System (Fig. 1B).

90 The Mesozoic stratigraphy of the study area is summarized in Figure 2. The Variscan basement is
91 unconformably overlain (D1 in Fig. 2) by the Triassic units deposited coeval to the initial stages of the
92 Mesozoic rifting. A regional angular unconformity is also common between the synrift Triassic and
93 postrift Jurassic sequences (San Román and Aurell, 1992; D2 in Fig. 2). The Jurassic sequence consists of
94 marine limestones and marls with variable overall thickness in the areas located north and south to the
95 South Cameros Fault. A nearly 1,000 m-thick marine Jurassic succession is recorded northwards

96 (Navarro-Vázquez, 1991), whereas south of this fault, the Jurassic is substantially reduced (c. 400 m-thick
97 near Bijuesca village). Marine Jurassic sedimentation ended with the lower Kimmeridgian reefal, oolitic
98 and bioclastic limestones of the Torrecilla Fm (Alonso and Mas, 1990). During the rest of the
99 Kimmeridgian the marine areas were progressively shifted eastwards into the Tethysian domains of the
100 Maestrazgo Basin (e.g., Bádenas and Aurell, 2001; Aurell et al., 2019a), resulting in the mid-
101 Kimmeridgian regional prerift unconformity (D3 in Fig. 2).

102 The uppermost Jurassic–Lower Cretaceous synrift succession in the Torrelapaja Subbasin studied here
103 consists of up to 500 m-thick siliciclastic and carbonate deposits that have been assigned to the Bijuesca,
104 Ciria, Torrelapaja and Escucha formations (Fig. 2), following the lithostratigraphy used in previous
105 regional studies (Schudack, 1987; Martín-Closas, 1989; Guimerà et al., 2004). The age of the lower units
106 was constrained by ostracod and charophyte biostratigraphy by Martín-Closas (1989) and U. Schudack
107 and M. Schudack (2009), respectively. The Bijuesca and Ciria formations developed within the Tithonian–
108 middle Berriasian, whereas the Torrelaja Fm was assigned to the latest Hauterivian–early Barremian age.
109 An uppermost Albian regional unconformity separates the studied synrift sequences from the postrift
110 Upper Cretaceous successions (D4 in Fig. 2), which include the continental sandstones and mudstones of
111 the uppermost Albian–middle Cenomanian Utrillas Fm (up to 270 m in thickness), followed by the 450–
112 550 m-thick shallow marine Cenomanian–Campanian carbonate units (Alonso et al. 1993; García et al.,
113 2004).

114

115 3. MATERIALS AND METHODS

116 The reconstruction of the sedimentary evolution of the Torrelapaja Subbasin reported here is based on
117 stratigraphical, sedimentological, structural and palaeontological data acquired following extensive field
118 work, geological mapping and logging, complemented with a review of the published information. The
119 workflow relevant to this research consisted of: (1) structural analysis and geological mapping with a

120 combination of fieldwork and analysis of high-resolution aerial imagery; (2) stratigraphical and
121 sedimentological analysis based on logging of the synrift uppermost Jurassic–Lower Cretaceous
122 successions in selected outcrops (see Fig. 3 for location), supplemented by petrographical analysis of rock
123 hard samples (limestones, sandstones) in thin sections and by mineralogical composition of muddy
124 lithologies; (3) palaeontological fieldwork including the recovery of macrovertebrate remains by surface
125 collection, the microfossil sampling of muddy lithologies in selected fossil-bearing horizons, and location
126 within the geological framework of the new and previously described dinosaur fossil sites; and (4) review
127 and integration of data sets, that resulted in the delineation of updated regional maps showing the
128 palaeogeography of the Northeast Iberia at significant time intervals.

129 The dinosaur bearing-horizons have been sampled for the analysis of their micropaleontological content
130 (screen-washed samples of 2–5 kg). Moreover, three well-preserved oyster shells found in the upper part
131 of the synrift succession in the Bigornia trough were sampled for strontium-isotopic analysis. The
132 $^{87}\text{Sr}/^{86}\text{Sr}$ isotopes were determined with a TIMS-Phoenix thermal ionization mass spectrometer at the
133 *CAI Geocronología y Geoquímica Isotópica* of the *Universidad Complutense de Madrid* (Spain). Isotopic
134 data were corrected for possible ^{87}Rb interferences and were normalised to a value of 0.1194 for
135 $^{87}\text{Sr}/^{86}\text{Sr}$ in order to correct possible mass-fractionation. During the period of analysis, the NBS-987
136 standard gave an average $^{87}\text{Sr}/^{86}\text{Sr}$ value of 0.710245 ± 0.000019 , which was used to correct the
137 measured values from a possible deviation referred to the standard. The analytical error of the $^{87}\text{Sr}/^{86}\text{Sr}$
138 ratio referred to 2σ was 0.01%.

139

140 **4. STRATIGRAPHIC REMARKS AND STRUCTURE OF THE TORRELAPAJA SUBBASIN**

141 The geological mapping of the area including the Torrelapaja Subbasin (Figs. 3 and 4) shows the
142 distribution of lithostratigraphic units and main structural elements. The subbasin is bounded to the

143 northeast by the southwest-dipping Malanquilla Fault and, to the southwest, by the northeast-dipping
144 Carabantes Fault System (Carabantes Fault; Guimerà et al., 2004). The northeast-dipping Berdejo Fault
145 (or Cardejón Fault in Guimerà et al., 2004) separates the northern and southern Bigornia and Bijuesca
146 troughs. The uppermost Jurassic (Tithonian)–Lower Cretaceous sedimentary succession of the
147 Torrelapaja Subbasin characterized in this work is arranged in three synrift sequences bounded by major
148 unconformities that can be traced across the study area (Fig. 2): (1) synrift sequence-1 (SS-1) includes the
149 alluvial deposits of the Bijuesca Fm and the lacustrine to palustrine limestones of the Ciria Fm; (2) synrift
150 sequence-2 (SS-2) is formed by the mixed siliciclastic and carbonate continental succession of the
151 Torrelapaja Fm; (3) synrift sequence-3 (SS-3) is characterized by a transitional continental to marine
152 succession, with oyster-rich sandy-limestones with abundant plant debris, followed by coal-bearing
153 sandstones and shales typical of the Escucha Fm. Selected key field views of the synrift units and
154 bounding surfaces in the Bijuesca (Fig. 5) and in the Bigornia troughs (Figs. 6 and 7) are provided.

155 The lower boundary of SS-1 is the subaerial exposure surface developed on top of the prerift Jurassic
156 marine limestones. This discontinuity has an associated stratigraphic gap encompassing at least the late
157 Kimmeridgian. The individualization of the Torrelapaja Subbasin as a depositional area began with the
158 sedimentation of SS-1. The sequence includes two vertically and laterally related continental units: the
159 alluvial conglomerates, sandstones and mudstones of the Bijuesca Fm, and the palustrine-lacustrine
160 limestones of the Ciria Fm (Fig. 5A). Most of the normal faults that were active during sedimentation of
161 SS-1 are NW-SE trending. Moreover, the northwestern Bigornia trough is compartmentalized by an
162 additional set of normal faults with perpendicular orientation (NE-SW). In the uplifted blocks, SS-1 is very
163 reduced and fossilizes normal faults affecting the marine Jurassic units (Fig. 4A-B; see also Alonso and
164 Mas, 1988, 1990; Sacristán-Horcajada et al., 2012). In the most subsident areas of the northwestern
165 Bigornia and Bijuesca troughs (Fig. 4A-C), the unit form thick successions (up to 350–400 m; see also
166 Alonso and Mas, 1990 and Sacristán-Horcajada et al., 2011, 2012), and the erosive gap of the underlying
167 marine Jurassic rocks is reduced. There, the lower boundary of SS-1 is generally a low-relief

168 paraconformity developed on top of the lower Kimmeridgian Torrecilla Fm (Fig. 5C). In the less subsident
169 areas of the southeastern Bigornia trough, the basal conglomerates of the Bijuesca Fm are 0–30 m-thick
170 and the sequence is dominated by the limestones of the 20–80 m thick Ciria Fm.

171 The lower boundary of SS-2 (Torrelapaja Fm) is the major unconformity between the lacustrine
172 limestones of the Ciria Fm (lower-middle Berriasian) and the continental terrigenous of the Torrelapaja
173 Fm (uppermost Hauterivian-lower Barremian). An irregular incised (some dm's in deep) karstic surface is
174 frequently observed on top of the lacustrine limestones of SS-1 (Figs. 6A and 7A). The karstic cavities are
175 filled by argillaceous mudstones, which may include a rich assemblage of disarticulated vertebrate
176 remains (see section 6). Angular unconformities are commonly observed in the southeastern Bigornia
177 trough, where some of the NE-SW faults that were active during the sedimentation of SS-1 are fossilized
178 by SS-2 (Fig. 8). The Torrelapaja Fm (SS-2) includes a high variety of continental facies, mainly muddy
179 facies (from shales to calcareous mudstones) and intercalated limestones, conglomerates and
180 sandstones (Figs. 6C–F and 7D). The unit reaches maximum thickness of 60–80 m in the southeastern
181 Bigornia trough (Fig. 4B). By contrast, the unit is absent or very reduced in the southern Bijuesca trough
182 and in the northwestern edge of the Bigornia trough, where the postrift sandstones of the Utrillas Fm
183 usually overlay the SS-1 (Fig. 5A).

184 The lower boundary of SS-3 is a regional angular unconformity, which locally fossilizes normal faults that
185 were active during sedimentation of previous sequences (Fig. 3). SS-3 may directly overlay SS-1, as
186 observed in the northwestern part of the Bigornia trough, in the outcrops located south of Ciria (Fig.
187 4A; see Alonso and Mas, 1988; Guimerà et al, 2004). The Escucha Fm (SS-3) is only found in the Bigornia
188 trough. Maximum thickness of the unit measured northeast of Berdejo village is around 50 m. There, the
189 unit consists of shales and burrowed micaceous sandstones rich in plant remains, with intercalation of
190 sandy skeletal limestones and abundant oyster debris (Fig. 7E-F). Its upper part is poorly exposed or
191 eroded across the Torrelapaja Subbasin and consists of sandstones and shales with interbedded coal

192 (lignite) levels. Lignite levels of the Escucha Fm were quarried south of Ciria village, in Vallehermoso (Fig.
193 4A). A borehole in this locality revealed the presence of a 33 m-thick succession of shales and siltstones
194 including intercalation of dm- to m-thick lignite beds (IGME, 1984). In its type locality, the Escucha Fm
195 has a similar lithological evolution, with a lower member dominated by sandy skeletal (oyster rich) levels
196 and a middle-upper part with abundant lignite levels (e.g., Querol et al., 1992). The upper boundary of
197 SS-3 is the major angular unconformity, which involved block tilting and erosion previous to the
198 deposition of the postrift deposits. The postrift Utrillas Fm rests on a low-angle unconformity and
199 fossilizes normal faults that were active during the sedimentation of the previous synrift sequences, as
200 observed east of Torrelapaja (Fig. 4B) or south of Bijuesca (Fig. 4C).

201

202 **5. FACIES ANALYSIS: PALEOENVIRONMENTAL RECONSTRUCTION**

203 **5.1. Synrift sequence 1: Alluvial to palustrine-lacustrine systems**

204 The SS-1 sedimentary system has been characterized in the most complete Bijuesca log (Sacristán-
205 Horcajada et al., 2011), complemented with new data of Las Cañadas log, located in the southeastern
206 Bigornia trough (see LC1 and BJ logs respectively in Figs. 4B and C). Further information of the
207 sedimentary evolution of SS-1 in the northwestern Bigornia trough is provided in Sacristán-Horcajada et
208 al. (2012).

209 The terrigenous clastic succession of the Bijuesca Fm represents deposition from proximal to distal
210 alluvial fans (Fig. 9A). In Bijuesca, the lower part of the succession is dominated by fining-upward
211 sequences of matrix-supported conglomerates with sandstone and limestone clasts. Inverse grading is
212 also observed. These deposits were interpreted as debris flow deposits of proximal alluvial fans
213 (Sacristán-Horcajada et al., 2011). The middle part of the Bijuesca Fm consist of clast-supported
214 conglomerates with cm-sized limestone pebbles and normal grading, fining-upward to cross-bedded

215 sandstones and red mudstones (Fig. 5F, G) deposited in channels and flood plains of middle alluvial fan
216 areas. Red mudstones with local root traces and intercalated cross-bedded sandstones dominate in the
217 upper part of the unit and represent deposition in a distal alluvial fan. Mudstones and nodular
218 (bioturbated) limestones with characean algae and gastropods at the topmost part of the unit indicates
219 the setting of carbonate palustrine subenvironments. The new dinosaur fossil site of La Atalaya occurs in
220 a palustrine level found at this topmost part, in the transition to the overlaying Ciria Fm (Fig. 5A-B; see
221 section 6).

222 During SS-1 there was an expansion of the lacustrine system of the Ciria Fm over the alluvial fans of the
223 Bijuesca Fm. The Ciria Fm was interpreted as a low-gradient ramp margin lake, mostly sourced from
224 spring waters (Sacristan-Horcajada et al., 2011). Carbonate saturated waters could be related to
225 discharges from karstic aquifers sourced from the Jurassic marine limestones. The Ciria Fm is
226 characterized by meter-thick sequences from lacustrine to palustrine facies (Fig. 9A-B). Lacustrine facies
227 encompass tabular meter-thick bioclastic limestones with characean algae, ostracods, gastropods and
228 bivalves. Limestones with bioclastic lime mudstones and wackestones represent deposition in low-
229 energy lacustrine areas. Bioclastic wackestones to packstones with intraclasts, quartz grains and black
230 pebbles formed in littoral to shallow lacustrine areas. The palustrine facies corresponds to
231 nodular/brecciated limestones bearing similar skeletal components than the lacustrine limestones, but
232 including evidences of edaphic processes (e.g., nodulization, brecciation, root traces, black pebbles,
233 fenestral porosity; Fig. 9C). The palustrine-lacustrine facies also include gray mudstones and marls and
234 local oncolitic limestones with cm-thick oncoids with bioclastic cores in Las Cañadas log (Fig. 9B-D).

235 In Las Cañadas the Ciria Fm includes sandstones and clast-supported conglomerates with sharp flat or
236 channelized bases and limestone pebbles. Their intercalation within the palustrine-lacustrine facies
237 reflects deposition in the distal alluvial fan area, with sheet flood deposits or channelized flows entering
238 in the lake.

239 5.2. Synrift sequence 2: Distal alluvial fans and shallow lakes

240 Facies analysis of sequence SS-2 (Torrelapaja Fm) is mainly based on the data collected in three logs
241 located in the eastern subsident areas of the Bigornia trough (see LC, VT and VJ logs in Fig. 4B). Three
242 terrigenous muddy facies have been differentiated based on colour and mineralogy (Fig. 10). Ochre to
243 purple mudstones and ochre to violet marlstones/calcareous mudstones include levels rich in Fe-pisoids
244 and root traces/hydromorphic soils and local reworked skeletal debris (ostracods, charophytes and
245 vertebrate remains). They represent deposition in distal alluvial plains with local vegetated areas and
246 lateritic soils. These facies are similar to those found in lateritic palaeosoils in age-equivalent units
247 characterized in the southern Maestrazgo Basin, as in the lower Blesa Fm (Oliete Subbasin: Laita et al.,
248 2020). In contrast, gray marlstones/calcareous mudstones have more abundant ostracods, charophytes
249 and plant debris and some reworked Fe-pisoids, and preferentially accumulated in palustrine to shallow
250 lacustrine areas.

251 Limestones include a high variety of palustrine to shallow lacustrine facies (Fig. 11A). Bioclastic and
252 fenestral bioclastic limestones (wackestones/packstones, occasional grainstones) with abundant
253 bivalves, gastropods, ostracods and characean algae and some quartz grains (silt to medium sand),
254 dominate. The bioclastic limestones encompass subfacies with accumulated broken bivalves and
255 gastropods (Fig. 11B) or ostracods (Fig. 11C), both produced by hydrodynamic sorting by high-energy
256 events in lacustrine subenvironments. Other group of subfacies is dominated by ostracod and
257 charophytes deposited in quiet lacustrine areas (Fig. 11D). The fenestral bioclastic limestones with
258 abundant microcracks and root traces formed in palustrine areas (Fig. 11E). Two additional grain-
259 supported facies, tufa limestones and intraclastic/litoclastic sandy limestones are also present (Fig. 11A).
260 Tufa limestones include oncolitic subfacies with entire and broken oncoids (up to few cm-size) and
261 intraclasts (bioclastic facies, phytoclasts) in the matrix (Fig. 11F), as well as phytoclastic subfacies with
262 mm- to cm-size clasts of coated plant stems and stromatolites, oncoids and oncolid fragments (Figs. 6F

263 and 11G). The tufa limestones formed in palustrine-lacustrine areas as indicated by their intercalation
264 within gray marlstones/calcareous mudstones (Fig. 11A). The intraclastic/litoclastic facies is a mixture of
265 poorly sorted and variably rounded grains, including mm- to few cm-size lithoclasts (quartzite and
266 Jurassic limestones), intraclasts (e.g., muddy and bioclastic facies), oncolid fragments and quartz sand
267 grains (Fig. 11A). Nature of grains and lenticular geometries with channelized bases indicate deposition
268 by high-energy floods carrying lithoclasts from emerged areas and eroding both distal plain and
269 palustrine-lacustrine deposits.

270 Conglomerates and sandstones appear both as isolated tabular or lenticular beds and bed packages (dm
271 to few m-thick). The conglomerates are clast-supported with subangular to subrounded clasts up to 10
272 cm in size and granule to sand matrix. They have usual channelized bases, planar- and trough cross
273 bedding, cross- and parallel lamination, and normal gradation (Fig. 6E). Conglomerates with quartzite
274 (Paleozoic) and limestone (Jurassic) clasts dominate in the eastern section (Valdelavieja), intercalated
275 within distal alluvial plain facies (Fig. 11A). In contrast, conglomerates including only quartzite clasts are
276 recorded in Valdelatorre log. Fine to medium quartz sandstones have usual planar- and trough cross
277 bedding, cross- and parallel lamination, local ripples (Fig. 6C) and bioturbation (vertical traces).
278 Sandstones occasionally include coarse grains (quartzite and limestone clasts, intraclasts of lacustrine-
279 palustrine facies, Fe-pisoids, oncolid fragments) and bioclasts (bivalves, charophytes, ostracods). The
280 vertical relationships of sandstones and conglomerates with terrigenous muddy facies indicates that they
281 represent channels in middle-distal alluvial plain, reaching also subaqueous palustrine-lacustrine areas.
282 In turn, the isolated packages of conglomerates with quartzite clasts (Fig. 11A) indicate a different source
283 and are interpreted as channels of ephemeral braided streams within the plain.

284 The described facies have a lateral and vertically preferential distribution, which allow differentiating
285 three sedimentary stages (Figs. 10A and 12). Argillaceous Stage 1 corresponds to the sedimentary infill
286 on the paleokartic surface developed in the boundary between SS-1 and SS-2. It is dominated by muddy

287 facies of argillaceous composition (Fig. 11B) deposited in a distal alluvial plain with vegetated areas and
288 local lateritic soils. Lacustrine-palustrine areas comprise several vertebrate fossil sites (see section 6).
289 Carbonate-dominated Stage 2 reflects a rise in water level that led to the expansion of lacustrine-
290 palustrine areas and the increase in carbonate content in the distal plain (marlstone/calcareous
291 mudstones: see Fig. 10B), but also a coeval record of alluvial clastic input (sandstones) roughly from the
292 north and south (Figs. 11 and 13). In Stage 3, increase of terrigenous-clastic input resulted in the setting
293 of an asymmetrical sedimentary system. Southwards, middle-distal alluvial fan channels (conglomerates
294 with quartzite and limestone clasts, sandstones and muddy facies of predominant siliceous composition:
295 Fig. 10B) developed, and there was a significant reduction of lacustrine-palustrine areas to ponds. The
296 northern area was dominated by an alluvial-fluvial plain with terrigenous mudstone facies and with
297 ephemeral braided streams (conglomerates with quartzite pebbles).

298 **5.3. Synrift sequence 3: coastal sedimentation**

299 The Escucha Fm has been logged and sampled in an outcrop located south of Valdelavieja, where a
300 relatively thick succession (50 m) has been preserved from the post-rift erosion (Fig. 13A). There, the
301 Escucha Fm is dominated by yellowish to brown mudstones with dm- to m-thick intercalations of sandy
302 bioclastic limestones and sandstones. The terrigenous mudstones are mostly covered, but local small
303 outcrops allow to identify bivalves (including *Trigonia* bivalves and oyster shells of *Exogyras*) and thin
304 (few cm) levels rich in plant debris. The interbedded sandy bioclastic limestones (packstones) have
305 variable proportions of oyster fragments, whole and fragmented gastropods and serpulids, and quartz
306 grains (fine to medium sand). There are also echinoids spines, ostracods, brachiopods, carbonaceous
307 debris and both muddy and sandy intraclasts (Figs. 7F and 13B). The bivalve (oyster) sandy (quartz sand
308 grains) limestones are packstones characterized by accumulated debris of oysters, together with few
309 serpulids, gastropods and carbonaceous debris (Fig. 13C). These two facies have common bioturbation
310 with sedimentary infill consisting of silty lime mudstone texture. The top of the beds can be encrusted

311 and ferruginous, with frequent pholadid borings. Fine-grained sandstone beds with cross bedding and
312 cross- and parallel lamination are locally intercalated within the limestones. They contain lithic peloids in
313 the matrix and few bivalve debris.

314 Deposition of plant-rich terrigenous mudstones took place in low-energy terrestrial-coastal areas with
315 certain vegetal cover. Episodic marine flooding is indicated by the presence of levels with marine
316 bivalves. The sandy bioclastic limestones and sandstones represent deposition in a marine (probably
317 restricted embayed) area colonized mainly by oysters, gastropods and serpulids, and/or due to high-
318 energy events (storms) carrying quartz sand and skeletal debris from the open marine area.

319 Hydrodynamic sorting probably controlled the deposition of carbonate-rich and sandy beds, from well-
320 sorted accumulations of oysters in the bivalve sandy limestones, to poorly sorted sandy bioclastic
321 limestones with muddy and sandy intraclasts, to finer-grained sandstones. Bioturbation recorded in
322 limestones took place after the high-energy events.

323

324 **6. DINOSAUR FOSSIL SITES: DESCRIPTION AND STRATIGRAPHIC SETTING**

325 During the course of this investigation four new fossil dinosaur sites have been found. The *La Atalaya*
326 *site*, located 500 m southwest of Bijuesca village (see LA in Fig. 3), is up to now the only occurrence from
327 SS-1. The other three sites including dinosaur remains have been found in the lowermost levels of SS-2,
328 in the distal alluvial muddy facies (stage 1) that fills the irregular karstic surface developed on top of Ciria
329 Fm (Figs. 10A and 12A). The *Corrales de Valdelavieja site* is located about 2 km to the northeast of
330 Berdejo (see CV in Figs. 4B and 10A). The *Corrales de Las Cañadas site* is found 1.5 km northeast of
331 Torrelapaja village (see CC1 in Fig. 4B). The *Valdelatorre site* is located 1.7 km east from Torrelapaja
332 village (see VT in Fig. 4B and 10A). In this section we provide a brief description of their fossil content.
333 Besides, the data reported here have allowed to precise the stratigraphic setting of some previously-
334 known sites from the Bigornia trough (Royo-Torres et al., 2012; Rey-Martínez and Royo-Torres, 2014).

335 The *La Atalaya fossil site* yields a large-sized limb bone fragment and other large-sized caudal vertebra
336 assigned to Sauropoda indet. (Fig. 5D-E). Other vertebrate remains recovered by surface collection are
337 an archosaur rib fragment and some crocodylomorph osteoderms. The marly levels found in this
338 fossiliferous interval also hosts a microfossil assemblage including charophytes (poracharaceans),
339 ostracods (cyprideans), gastropods (planorbids and other two taxa), archosaur teeth (mainly
340 crocodylomorphs) and eggshells. This site is included in a bed of palustrine nodular limestone facies
341 found at the uppermost part of the Bijuesca Fm (Figs. 5A-B and 9A). Edaphic process linked to root
342 bioturbation produce nodulization and brecciation of these palustrine facies. However, the nodular
343 limestone of the fossiliferous site is in detail a laterally discontinuous carbonate conglomerate with
344 rounded clasts (Fig. 5D) produced by remobilization, transport and accumulation of the nodules and
345 breccia generated by the edaphic processes. This conglomerate bed laterally passes to marls with root
346 traces. Its location in the topmost part of the Bijuesca Fm points towards its age is around the Tithonian-
347 Berriasian transition. The Bijuesca Fm is assumed to be mostly Tithonian in age, although the precise
348 location of the Tithonian-Berriasian boundary within this unit is uncertain (Martín-Closas, 1989). The
349 early-middle Berriasian age of the overlying Ciria Fm is locally constrained by charophyte
350 biostratigraphy (Martín-Closas, 1989), particularly by the association of *Atopochara trivolvis* var. *horrida*
351 and *Nodosoclavator bradleyi* found in the upper part of this unit (see Fig. 4A for location of the sampled
352 point).

353 The *Corrales de Valdelavieja fossil site* (lowermost Torrelapaja Fm) includes two theropod vertebrae (Fig.
354 6B) plus other indeterminate remains found in close contact to the karstic surface within the first stage
355 of muddy infill of the palaeokarst (ochre to red marlstones/calcareous mudstones; Fig. 10A). An
356 ornithopod (iguanodontian) tooth was also recovered from the overlying intraclastic/litoclastic sandy
357 limestone. In addition, an isolated spinosaurid theropod tooth crown, which is slightly lateromedially
358 compressed and ornamented with longitudinal ridges was found *ex-situ* in a boulder of
359 intraclastic/litoclastic facies that forms part of the infill of the paleokarst. Terrigenous muddy facies filling

360 the palaeokarst (see sample CV1 in log VJ2, Fig. 10A) also includes a microfossil assemblage with latest
361 Hauterivian–early Barremian charophyte remains (*Atopochara trivolvis ancora*, *A.t. triquetra*, *Globator*
362 *maillardii* var. *trochiliscoides*), ostracods (cyprideans and other unidentified groups), eggshell fragments,
363 lissamphibian bone fragments and gastropods. Above this interval, samples CV2 and CV3 and has yielded
364 an early Barremian charophyte association with *Atopochara trivolvis* var. *triquetra* (typical form),
365 *Clavator harrisii* var. *harrisii*, *Clavatoraxis* sp and *Charaxis* (see VJ2 log in Fig. 10A and Fig. 6A for sample
366 location).

367 In the *Corrales de Las Cañadas fossil site* (lowermost Torrelapaja Fm), a set of isolated macrovertebrate
368 remains was found within the first stage of infill of the paleokarstic surface (ochre to red mudstones: Fig.
369 10A). The most significant fossil material comprises a sauropod humerus (Fig. 7B), a fragmentary
370 theropod ilium, and a saurischian vertebral centrum. Other indeterminate remains were found *ex situ*,
371 possibly eroded from the karstic infill. A poor microfossil assemblage of latest Hauterivian–early
372 Barremian age has been identified in this level (see sample LC1 in log LC, Fig. 10A). It includes remains of
373 ostracods (mainly cyprideans) and scarce charophytes (utriculi of *Atopochara trivolvis ancora* and *A.t.*
374 *triquetra*), some of them showing reworking features.

375 In the *Valdelatorre fossil site* (lowermost Torrelapaja Fm) an ornithopod vertebra was found *ex-situ*, very
376 close to the palaeokarstic surface developed on top of the Ciria Fm. Therefore, it is not possible to
377 ascertain whether it comes from the palaeokarst infill or was eroded from the overlaying muddy/marly
378 levels. The sediment sampling in a gray marlstone/calcareous mudstone bed on top of the vertebrate-
379 bearing bed (see VT1 microfossil sample in log VT, Fig. 10A) allowed to characterize an early Barremian
380 charophyte assemblage dominated by abundant utriculi of *Atopochara trivolvis triquetra* (typical form)
381 along with thalli of *Clavatoraxis* sp. Also frequent are ostracods (several taxa, including cyprideans),
382 eggshell fragments and microvertebrate remains dominated by undetermined lissamphibian bone
383 fragments along with crocodylomorph teeth (bernissartiids and goniopholidids). Moreover, osteichthyan

384 remains are present in less abundance (teeth of *Lepisosteiformes* and *Amiiformes*, and ganoid scales).
385 The composition of this microfossil assemblage resembles to those of other lower Barremian successions
386 reported in alluvial to shallow lacustrine settings from the Iberian Basin (e.g., Gasca et al., 2017).
387 In the area of Corrales de Valdelavieja and Valdelatorre, additional vertebrate sites were previously
388 reported by Royo-Torres et al. (2012) and Rey-Martínez and Royo-Torres (2014). These authors found
389 ornithopods and isolated remains of theropod and sauropod dinosaurs from five different sites named
390 BJ-1 to BJ-5 (see Figs. 4B and 10A for location of the most significant BJ1 and BJ5 sites). In particular,
391 Royo-Torres et al. (2012) described cranial and postcranial material of an ornithopod specimen in BJ-1
392 site, and their phylogenetic analysis consider it as a basal styracosternan. This site is found in meter 27 of
393 the VT log, towards the lower part of the Torrelapaja Fm (see Figs. 6D and 10A). Rey-Martínez and Royo-
394 Torres (2014) describe a distal end of a sauropod tibia in BJ-5 site, which is located 1 m above the base of
395 the Torrelapaja Fm (see VJ2 log in Fig. 10A). The authors assumed that all the BJ sites were included in
396 the Ciria Fm, and were “Tithonian and with some doubt Berriasian” in age. However, the review of these
397 fossil sites show that they are actually included in the lower part of the Torrelapaja Fm, and are
398 therefore early Barremian in age.

399

400 **7. AGE OF SYNRIFT SEQUENCES AND REGIONAL CORRELATION**

401 Below we review the age of the three identified synrift sequences based in previous information and
402 new data obtained in this work. According to the age assignment provided, the possible equivalence of
403 the sequences defined in the Torrelapaja Subbasin to the units defined in the depocentral areas of the
404 Cameros Basin and in the western domains of the nearby Maestrazgo Basin is proposed and discussed
405 (Fig. 14).

406 **7.1. Synrift sequence 1: Tithonian-middle Berriasian**

407 As indicated above, relevant data to precise the age of SS-1 is the presence of an early-middle Berriasian
408 charophyte association found in the upper part of the Ciria Fm with *Atopochara trivolis* var. *horrida* and
409 *Nodosoclavator bradleyi* (Martín-Closas, 1989). Moreover, U. Schudack and M. Schudack (2009)
410 identified a rich Berriasian ostracod association, with different species of *Cypridea*, *Theriosynoecum*,
411 *Mantelliana* and *Darwinula* that points to freshwater environments for the sedimentation of the Ciria
412 Fm. Accordingly, at least the upper part of the of SS-1 (Ciria Fm) was coeval to the sedimentation of the
413 lower-middle Berriasian depositional sequence (Oncala Gr) defined in the Cameros Basin (DS-III in
414 Clemente, 2010; DS-3 in Quijada et al., 2013 and Mas et al., 2019).

415 The facies evolution recorded in the Torrelapaja Subbasin during the sedimentation of SS-1 (from alluvial
416 fan clastics to lacustrine limestones) shows that this unit corresponds to a single depositional sequence.
417 If a sequence-to-sequence correlation is done, SS-1 would be equivalent to the DS-III (Oncala Gr) of the
418 Cameros Basin. However, the particular tectono-sedimentary evolution of the Torrelapaja Subbasin
419 compared to the depocentral areas of the Cameros Basin leaves open the possible equivalence of the
420 lower part of the SS-1 to older Tithonian depositional sequences defined in the Cameros Basin (i.e. Tera
421 Group; DS I-II in Clemente, 2010 or DS 1–2 in Mas et al., 2019). In Figure 14 we suggest the possible
422 equivalence of the lower part of SS-1 with the DS-II (upper Tera Group), as previously proposed in
423 Sacristán-Horcajada et al. (2012).

424 **7.2. Synrift sequence 2: uppermost Hauterivian-lower Barremian**

425 The data reported here give further support to the latest Hauterivian–early Barremian age proposed for
426 the Torrelapaja Fm in previous works. Martín-Closas (1989) found a latest Hauterivian-earliest Barremian
427 association with *Atopochara trivolis triquetra* (primitive form), *Globator maillardii* var. *trochiliscoides*
428 and *Clavator calcitrapus* in an isolated outcrop of the Torrelapaja Fm located south to Ciria village (see
429 Fig. 4A for location of the sampled point). U. Schudack and M. Schudack (2009) also report in a rich-
430 assemblage of Hauterivian-early Barremian freshwater ostracods, including different species of *Cypridea*,

431 *Theriosynoecum*, *Fabanella*, *Mantelliana* and *Darwinula* genera. As indicated above (section 6), the
432 analysis of the lowermost levels of Torrelapaja Fm in Valdelavieja and Las Cañadas logs has yielded a
433 microfossil assemblage with utriculi of *Atopochara trivolvis* var. *ancora* and *A.t.* var. *triquetra* varieties,
434 and *Globator maillardii* var. *trochiliscoides* (samples LC1 and CV1, Fig. 10). Moreover, the marly levels
435 found in the lower part of the Torrelapaja Fm in the Valdelavieja-Valdelatorre area has yielded an early
436 Barremian charophyte association with abundant *Atopochara trivolvis* var. *triquetra* (typical form)
437 (samples VT1, CV2 and CV3, Fig. 10).

438 According to Martín-Closas (1989) and Clemente (2010), the Torrelapaja Fm was deposited coeval to the
439 lower part of the Enciso Group (Fig. 14). However, the age of the Enciso Group has been debated (see
440 Martín-Closas, 1989; U. Schudack and M. Schudack, 2009; Clemente, 2010; Suárez-González et al., 2013;
441 Moreno-Azanza et al., 2016; Muñoz et al., 2020). The late Hauterivian-Barremian age range assigned by
442 Clemente (2010) for the Enciso Group is coherent with the presence of *Atopochara trivolvis triquetra* in
443 the Enciso locality (Schudack, 1987), the abundant late Valanginian–Barremian ostracod association
444 found in the unit (U. Schudack and M. Schudack, 2009), and the presence of the Barremian–Albian
445 dasycladalean *Salpingoporella urladanasi* in the Leza Fm, a lateral equivalent of the Enciso Group
446 including levels with marine fossils (Suarez- González et al., 2013). Recently, Muñoz et al. (2020) propose
447 a mid-Hauterivian to mid-Barremian age range for the Enciso Group based in cyclostratigraphy, with the
448 obtained astrochronological scale fitting within the available biostratigraphic data.

449 **7.3. Synrift sequence 3: middle-upper Albian**

450 In the Bigornia trough, the SS-3 consists of shales and sandy skeletal (oyster-rich) limestones, which
451 grades upwards to a terrigenous mudstone dominated succession with interbedded coal levels. Despite
452 the poor exposure of the SS-3 across the studied area, there is no evidence indicating the existence of a
453 significant sedimentary discontinuity (or angular unconformity) within this succession, that have been
454 assigned here to the Escucha Fm. However, previous work in Bigornia trough (Alonso and Mas, 1988,

455 1993) considered the presence of a sedimentary discontinuity between the lower (oyster-rich) and upper
456 (coal-rich) successions. The authors suggested an early Aptian age for the oyster-rich succession, based
457 in its tentative correlation to the shallow marine units found more than 120 km southwards to the
458 Torrelapaja Subbasin, in the Maestrazgo Basin. This early Aptian age assignment was also assumed in
459 latter works (e.g., Guimerà et al., 2004; Mas et al., 2004; Suarez-González et al., 2013).

460 There are few exposures of Lower Cretaceous marine units exposed close the Torrelapaja Subbasin. The
461 closest shallow marine succession of Grávalos is found 60 km north of Torrelapaja, in the footwall of the
462 North Cameros thrust. In Grávalos, a 50 m-thick mixed siliciclastic-carbonate succession with skeletal-
463 rich beds (oysters, foraminifera, serpulids, rudists, green algae, echinoderms) have yielded an association
464 of Albian benthic foraminifera with *Flabellamina alexanderi* and *Haplophragmium* sp. (Muñoz et al.,
465 1997). According to these authors, this skeletal-rich succession is conformably overlain by the shales and
466 sandstones with coal levels typical of the middle-upper Albian Escucha Fm. As observed in Torrelapaja,
467 the shallow marine succession of Grávalos is also overlain by the postrift unconformity (Utrillas Fm).

468 The SS-3 of the Torrelapaja Subbasin is regarded here as time-equivalent to the Albian succession of
469 Grávalos, and is therefore proposed to be deposited around the middle-late Albian times (Fig. 14). The
470 middle-late Albian age proposed here for the SS-3 in the Torrelapaja Subbasin based on its correlation to
471 the closest marine unit found in an equivalent stratigraphic position is coherent with strontium isotopic
472 data obtained in our work. The isotopic analysis of three oyster shells (*Exogyra*) found in a yellowish
473 terrigenous mudstone interval within the lower part of the SS-3 (see Fig. 4B for location of the sampling
474 site) have yielded $^{87}\text{Sr}/^{86}\text{Sr}$ isotopes values of $0.707447 \pm 2 \times 10^{-6}$, $0.707459 \pm 3 \times 10^{-6}$ and 0.707460 ± 3
475 $\times 10^{-6}$, respectively. Due to its deposition in coastal environments, these values obtained from oyster
476 shells may have abnormally high values reflecting a relatively more radiogenic isotopic signal linked to
477 freshwater input (e.g., Bryant et al., 1995). However, the significance of these strontium values is
478 supported by the similar results obtained from the three well-preserved shells analysed, which fit in turn

479 the expected isotopic Cretaceous values. Combining the age of the underlying Torrelapaja Fm
480 (uppermost Hauterivian-lower Barremian) and of the overlying Utrillas Fm (uppermost Albian-middle
481 Cenomanian: Alonso et al. 1993; García et al., 2004), and the global marine $^{87}\text{Sr}/^{86}\text{Sr}$ Cretaceous curve
482 (Bralower et al., 1997; Denison et al., 2003; McArthur et al., 2012), the obtained values are constrained
483 in two different time intervals: late Barremian-early Aptian and middle-late Albian respectively (Fig.
484 13D). However, the late Barremian-early Aptian age for the SS-3 sequence is unlikely considering not
485 only the major angular and erosive unconformity with the underlying uppermost Hauterivian-lower
486 Barremian SS-2 (Torrelapaja Fm), but also the overall palaeogeography of Northeast Iberia during Early
487 Cretaceous times (see discussion in section 9).

488

489 **8. TECTONO-SEDIMENTARY EVOLUTION OF THE TORRELAPAJA SUBBASIN: REGIONAL IMPLICATIONS**

490 As shown in the previous section, the uppermost Jurassic-Lower Cretaceous record of the Torrelapaja
491 Subbasin is very discontinuous, with sedimentation stages during the Tithonian-middle Berriasian
492 (Bijuesca and Ciria formations), the latest Hauterivian-early Barremian (Torrelapaja Fm), and the middle-
493 late Albian (Escucha Fm), respectively. The angular unconformities developed between the synrift
494 sequences and the onlap geometries (see Fig. 8) should be explained in a context in which deformation
495 and block tilting associated to faulting also occurred during the periods without sedimentary record in
496 the basin.

497 The evolution of the successive synrift stages recorded in the Torrelapaja Subbasin was mostly controlled
498 by the activity of the three major NW-SE trending extensional faults described above: the southwest-
499 dipping Malanquilla Fault, the northeast-dipping Berdejo Fault and the northeast-dipping Carabantes
500 Fault System (Figs. 3 and 15). The Bigornia trough is located very close (< 1-2 km) to the South Cameros
501 Fault (section 1-1'; Fig 15). It has an asymmetric graben geometry, tilted towards the Berdejo Fault (i.e.
502 towards the southwest). The Bijuesca trough, however, has a significant halfgraben geometry, which is

503 indicative of the listric geometry of the border Carabantes Fault System. The asymmetry of both
504 structures suggests their link in depth with the basal detachment of the Malache and South Cameros
505 faults, i.e. with the southeast Cameros Basin. Numerous minor normal faults affect the synrift series,
506 usually in a NW-SE direction and, especially in the Bigornia graben, also in other directions. The latter
507 commonly have a NE-SW direction and dips to the northwest (i.e. towards the Cameros Basin) producing
508 traverse halfgrabens, as those located 1-3 km south of the Ciria village, that highly compartmentalized
509 the Bigornia graben (section 2-2'; Fig. 15). The mapping of these three major faults, along with the
510 identification and other minor scale synsedimentary normal faults allow reconstructing the extension of
511 depositional domains and depocentral areas of the Bigornia and Bijuesca troughs during the
512 sedimentation of SS-1, SS-2 and SS-3 (Fig. 16).

513 During the sedimentation of SS-1, the activity of the Carabantes Fault System resulted in the formation
514 of the Bijuesca halfgraben, which record more than 200 m of continental deposits in its southern
515 depocentral areas (Fig. 16A). This halfgraben structure is suggested by the overlap of the Utrillas Fm
516 (postrift unconformity) on increasingly older units (Ciria and Bijuesca formations and even Upper Jurassic
517 rocks) towards the northeast, that is, towards the Berdejo fault (Fig. 3). The conglomerates of the
518 Bijuesca Fm were sourced by the uplifted marine Jurassic rocks. Palaeocurrent data measured in Bijuesca
519 indicates a source area located to the south (Fig. 16A). The analysis of the nature of limestone clasts of
520 the conglomerates in the well exposed outcrop of Bijuesca reveals a predominance of clasts derived
521 from the erosion of the Middle-Upper Jurassic units in the lower part of the Bijuesca Fm, whereas Lower
522 Jurassic clasts dominate in the conglomeratic beds of the upper part of the unit. This trend can be
523 related to the progressive denudation of the marine Jurassic rocks exposed in the southern uplifted
524 areas (i.e. inverted vertical clast distribution or *normal unroofing sequence*; Colombo, 1994). It is
525 interesting to note that the areas that remained uplifted in the southern margin of the Bijuesca trough
526 during the sedimentation of SS-1 show a very large erosive incision on the marine Jurassic rocks, and the
527 postrift Utrillas Fm overlays the lowermost Jurassic units (see the outcrops south of Bijuesca in Fig. 3).

528 The combined activity of the Berdejo and Malanquilla faults resulted in the formation of the NW-SE
529 trending Bigornia graben. The composition of the clast found in the conglomerates of the Bijuesca Fm in
530 this graben also indicates a dominant source from the surrounding uplifted marine Jurassic rocks.
531 Palaeocurrent data points to dominance of a southern drainage area at the onset of the sedimentation
532 of SS-1, followed by a northern source during the sedimentation of the middle and upper part of the
533 Bijuesca Fm (Fig. 16A; see Sacristán-Horcajada et al. 2012). Compared to the Bijuesca halfgraben,
534 thickness distribution in Bigornia graben is very irregular due to the activity of a set of NE-SW trending
535 faults (Figs. 15 and 16A). Moreover, the graben was asymmetric, with maximum thickness (c. 350–400
536 m) measured in the hanging wall of the Malanquilla Fault, but with a thicker sequence expected to occur
537 in the hanging wall of the Berdejo Fault according to structural reconstruction (section 1-1'; Fig. 15). The
538 posrift Utrillas Fm and younger units cover the unit in this area and it prevents the corroboration of this
539 assumption. A 180 m-thick succession was measured in the Berdejo fault zone, but it is located in its
540 southwesternmost fault block, which only recorded a small amount of the displacement of the Berdejo
541 Fault. Such outcrop of the Bijuesca and Ciria formations close to the fault, together with other very close
542 located in the footwall of the fault, clearly point that the sedimentation likely encompassed the entire
543 Torrelapaja Subbasin during this stage, and that the Berdejo and minor intrabasinal faults were only
544 responsible for the changes in thickness of the unit.

545 The lacustrine-palustrine carbonates of the Ciria Fm shows a large expansion across the entire
546 Torrelapaja Subbasin (Fig. 9). Discrete terrigenous-clastic of sandstones and clast-supported
547 conglomerates intercalated within the palustrine-lacustrine limestones of the Ciria Fm in less subsident
548 areas of the southeastern Bijuesca through (see log CC1 in Fig. 9B) are interpreted as distal alluvial fan
549 deposits sourced by the uplifted areas by the Malanquilla Fault.

550 During the sedimentation of SS-2 (Torrelapaja Fm), a set of normal faults with variable orientation was
551 active in the Torrelapaja Subbasin (Fig. 16B). The Malanquilla and Berdejo faults were reactivated and

552 controlled the evolution of the Bigornia trough. The angular unconformity between SS-1 and SS-2 in the
553 southeastern Bigornia trough shows evidence of previous faults that were not active during SS-2 (Fig. 8).
554 According to cartographic data, the set of NE-SW faults that compartmentalized the northwestern
555 Bigornia trough during the previous SS-1 were not reactivated (Fig. 3). However, the activity of these
556 faults should not be ruled out, because a set of faults with variable orientation (E-W to N-S) controlled
557 the sedimentation in the southeastern Bigornia trough (Fig. 16B). The reactivation of the NE-SW faults
558 located to the southeast (near the locality of Malanquilla) probably caused the displacement of the local
559 depocentres associated with intrabasinal halfgrabens towards that direction along the Bigornia trough
560 (see section 2-2': Fig. 15). In the southern Bijuesca through, the local sedimentation and preservation of
561 SS-2 has been related to some minor normal faults (see also Fig. 4C).

562 After the initial stage of irregular sedimentation at the onset of SS-2 (stage 1), there were two stages
563 with variations in depositional subenvironments, which can be partly linked to the tectonic activity (Fig.
564 12). Stage 2 records carbonate-dominated distal alluvial muddy flats (marlstones/calcareous mudstones)
565 with local lateritic soils and carbonate shallow lakes in central areas, and very local terrigenous input in
566 the northern and southern marginal areas. In contrast, Stage 3 encompasses a more terrigenous-clastic
567 and asymmetric system, characterized to the south by a middle-distal alluvial fan with sandstone and
568 conglomerate channels bearing both limestone (Jurassic) and quartzite (Paleozoic) clasts, and to the
569 central and northern parts by ephemeral braided streams of quartzite conglomerates and muddy flats
570 (siliceous mudstone). The increase of terrigenous-clastic supply from stage 2 to stage 3 can be related to
571 an increase of tectonic activity, with conglomerates sourced by nearby uplifted Mesozoic-Paleozoic rocks
572 (from the south-southeast) and the braided streams sourced from uplifted Paleozoic rocks located
573 eastwards to the Torrelapaja Subbasin (Fig. 16B).

574 The sedimentation of SS-3 (Escucha Fm) spreads over the northeastern marginal areas of the Bigornia
575 trough, with thickness around 50 m in the areas located close to the Malanquilla and Berdejo faults (Fig.

576 16C). The poor exposure of the unit does not allow to reach precisions on the synsedimentary fault
577 activity as in previous sequences. However, the existence of relatively thick accumulation of the coal-
578 bearing successions of the Escucha Fm south of Ciria (Vallehermoso locality: IGME, 1984) suggests the
579 reactivation of a new fault plane related to the Malanquilla Fault and located in the footwall of the
580 former one. There is no evidence of sedimentation of the SS-3 sequence in the Bijuesca trough where
581 the postrift Utrillas Fm unconformably overlay SS-1 or older marine Jurassic units (Fig. 3).

582 In the northwestern Bijuesca trough, SS-3 unconformably overlay with high angle (>30) the beds of the
583 Bijuesca and Ciria formations, as well as the NE-SW faults and halfgraben structures described for SS-1
584 south of Ciria (Figs. 3 and 15). Such geometrical disposition suggests the following evolutionary stages
585 (see section 1-1'; Fig. 15): (i) the overall tilting of the SS-1 and SS-2 and of the prerift sequence towards
586 the SW, (ii) an erosional stage that levels the structure, and (iii) the onset of the sedimentation of SS-3,
587 the latter being favoured by the activation of the new fault plane associated to the Malanquilla Fault. At
588 this stage, it is probably that the Bigornia trough could change in graben polarity, with the eastern
589 Malanquilla fault being in turn the master fault of the graben. Similar changes in polarity of faults have
590 been also described in the Maestrazgo Basin (Querol et al., 1992; Capote et al., 2002). The long period of
591 time between the deposition of SS-2 and SS-3 proposed in this work (Fig. 14) is coherent with such a
592 change in polarity in the Torrelapaja Subbasin.

593 To summarize, the three periods of sedimentation recorded in the Torrelapaja subbasin correlate well
594 with the periods of higher tectonic activity defined by subsidence analysis and regional data in the
595 Cameros and Maestrazgo basins for the Late Jurassic-Early Cretaceous rifting stage (Mas et al., 1993,
596 Salas et al., 2001; Liesa et al., 2006, 2019). This means that the record in this sub-basin is mainly
597 produced and preserved by the differential subsidence associated with the faults. Note how in many
598 cases the three synrift sequences are truncated and bounded by angular unconformities, and in turn are
599 truncated by the postrift unconformity. In fact, in many of the fault footwall blocks, the postrift Utrillas

600 Fm rests almost directly on the Jurassic prerift series (Figs. 3 and 15). This is coherent to the position of
601 this subbasin in a marginal area of sedimentation in relation to the depocentral area of the Cameros
602 Basin.

603 On the other hand, the complex geometry of the Torrelapaja Subbasin, mainly defined by two nearly
604 perpendicular fault sets acting simultaneously, greatly resembles what happens during the Late Jurassic-
605 Early Cretaceous rifting stage in the Cameros Basin and in the marginal subbasins of the Maestrazgo
606 Basin (Platt, 1990; Cortés et al., 1999; Liesa et al., 2006, 2018; Antolín-Tomás et al., 2007; Meléndez et
607 al., 2009; Aurell et al., 2016, 2018). Contemporary multi-directional normal fault activity points to a
608 regime of radial extension. The greater significance of faults in NW-SE direction with respect to those in a
609 NE-SW direction, which defines the main structuring of the Torrelapaja Subbasin in sedimentary troughs
610 (Bigornia and Bijuesca), with respect to those in a NE-SW direction suggests a direction of main NE-SW
611 extension and a secondary NW-SE extension, as it has also been proposed for the Cameros Basin from
612 the analysis of faults, calcite veins and magnetic susceptibility anisotropy (Guiraud and Séguret, 1984;
613 Marqués et al., 1996; García-Lasanta et al., 2014).

614

615 **9. DISCUSSION: THE PALAEOGEOGRAPHY OF NORTHEAST IBERIA REVISITED**

616 The data and review reported here have implications on the reconstruction of the overall
617 palaeogeography of the uppermost Jurassic–Lower Cretaceous Iberian Basin rift system, providing
618 arguments to precise previous reconstructions of Northeast Iberia.

619 The palaeogeographic maps of Figure 17 show the reconstruction around the early Berriasian, the early
620 Barremian and the middle Albian, thus for the three synrift sequences recorded in the Torrelapaja
621 Subbasin, respectively. The studied subbasin is located in the southeastern edge of the Cameros Basin,
622 relatively close to the northwestern Maestrazgo Basin (Fig. 1A). Figure 14 shows the equivalence

623 between the three synrift sequences recorded in the Torrelapaja Subbasin to those defined in the
624 marginal subbasins of the Maestrazgo Basin. It is noted that the stratigraphic gap associated to the
625 unconformity between the SS-1 and SS-2 in the Torrelapaja Subbasin fits a period of irregular and
626 discontinuous sedimentation both in the Cameros Basin (DS IV-V of Clemente, 2010), and in the
627 Maestrazgo Basin, which shows a gap of variable amplitude associated to the unconformity between the
628 major synrift sequences 1 (Tithonian–Berriasian) and 2 (Valanginian–lower Albian) defined in Liesa et al.
629 (2019).

630 **9.1. Early Berriasian palaeogeography**

631 In the Torrelapaja Subbasin, sedimentation around the Tithonian-Berriasian transition occurred in
632 alluvial fan systems, which grade upwards to the setting of carbonate palustrine-lacustrine environments
633 across the entire sedimentation areas during the Berriasian.

634 The depocentral areas of the Cameros basin during the Tithonian-middle Berriasian record the different
635 siliciclastic-carbonate formations of the up to 3,800 m-thick Tera and Oncala groups (Gómez-Fernández
636 and Meléndez, 1994). Around the Tithonian-Berriasian transition, the westernmost areas were
637 dominated by braided fluvial systems, that gradually evolved to meandering fluvial systems in the
638 western-central areas (Clemente, 2010). Northwards, these fluvial deposits graded progressively to
639 broad, low-gradient tidal flats traversed by shallow meandering channels. The laterally related
640 carbonate-evaporitic deposits found in the northeastern part of the basin of the lower-middle Berriasian
641 Oncala Group were deposited in saline mudflats, with large sulphate input derived from the episodic
642 incursion of marine waters (Quijada et al., 2013, 2020). Similar sulphur isotopic compositions recorded in
643 the carbonate-gypsum deposits of the Oncala Group and in the Basque-Cantabrian Basin support the
644 connection of the Cameros Basin with marine and transitional areas of the Basque-Cantabrian Basin
645 during Berriasian times (Quijada et al., 2013). The existence of marine incursions is further supported by
646 the presence of scarce miliolids in the eastern Cameros basin in the units deposited around the

647 Tithonian-Berriasian transition: in the Matute Fm (upper Tera Group, DS-II; Fig. 14) and in the upper
648 Oncala Group (Gómez-Fernández and Meléndez, 1994).

649 In the southeastern margin of the Cameros Basin, including the Torrelapaja Subbasin, the abundance of
650 the charophytes *Porochara* and *Mesochara* found in the Ciria Fm suggests the possible episodic setting of
651 brackish waters (Martín-Closas, 1989). The presence of brackish waters around this marginal area could
652 be related to ephemeral marine influence sourced from the north (Basque-Cantabrian Basin). The overall
653 palaeogeography of the Iberian Basin rift system during the Berriasian (Fig. 17A) with the marine
654 sedimentation areas confined to the eastern Maestrazgo Basin (e.g., Aurell et al., 2016, 2019b; Bádenas
655 et al., 2004, 2018; Liesa et al., 2019), makes unlikely an alternative marine source from the Tethysian
656 realm. Also of interest are the lacustrine-palustrine carbonates found eastwards to the Torrelapaja
657 Subbasin, in Ricla (Fig. 17A), which also include abundant *Porochara* and *Mesochara* (Martín-Closas,
658 1989). As proposed by Salomon (1982) these carbonates are regarded here as time counterparts of the
659 Berriasian Ciria Fm. However, this is a tentative correlation, because the recorded charophyte
660 association of Ricla does not provide conclusive information about its age (Martín-Closas, 1989; Soria et
661 al., 1995).

662 **9.2. Early Barremian palaeogeography**

663 During the early Barremian, most of the Cameros basin was the site of continental sedimentation (Fig.
664 17B). The fluvial systems that dominated the sedimentation in the south-central part of the basin
665 changed towards the northwest to small carbonate lakes, and towards the northeast to a siliciclastic and
666 carbonate-dominated continental setting (Clemente, 2010). Assuming an early Barremian age for the
667 Leza Fm (see discussion above), evidences of marine influence coeval to the sedimentation of the SS-2
668 would be recorded in the northeastern edge of the Cameros Basin, with the relatively abundant
669 presence of dasycladaleans, echinoderms and miliolids in some carbonate levels. The Leza Fm was
670 deposited in a system of coastal wetlands with both freshwater and seawater influence, laterally related

671 to the fluvio-lacustrine deposits towards the south (Suarez-González et al., 2013). Further evidence of
672 marine influence around the earliest Barremian is indicated by the presence of debris of echinoderms in
673 the siliciclastic-dominated succession of the Enciso Group logged close to Navalsaz village (Muñoz et al.,
674 2020; see Fig. 17B for location).

675 The discussion about the provenance of the episodic marine incursions to explain the presence of marine
676 skeletal-rich levels in the Enciso Group in the northeastern Cameros Basin can be further approached
677 with the available regional data. Lower Barremian deposits found in the Aguilón Subbasin (north to the
678 Maestrazgo Basin, Fig. 17B) correspond to the ostracod-rich lacustrine deposits of the Aguilón Fm (Fig.
679 14). In this unit, with the exception of a few *Fabanella boloniensis* (allowing more saline brackish water
680 environments), all identified species of ostracods indicates freshwater environments (U. Schudack and
681 M. Schudack, 2009). Further south, in the Oliete Subbasin, the presence of oyster-rich limestones in the
682 middle part of the Blesa Fm indicates the episodic marine connection with the open-marine areas of the
683 Maestrazgo Basin during the early Barremian (Fig. 17B; Aurell et al., 2018). However, there is no data
684 supporting that these marine incursions could reach the sedimentary domains located further north, in
685 the Aguilón Subbasin or in the eastern Cameros Basin. Similarly, the Artoles Fm in the Galve Subbasin
686 represented sedimentation in coastal to shallow marine environments, whereas towards the northwest,
687 in the Las Parras Subbasin, palustrine-lacustrine marls and limestones, containing fresh-water ostracods
688 and charophytes developed (Camarillas Fm: Fig. 14; Liesa et al., 2019). Moreover, considering that the
689 Barremian–Aptian marine facies are confined to the eastern areas of the Maestrazgo Basin (e.g., García,
690 1982; Liesa et al., 2019), the connection between the Tethys and the Cameros Basin during this time
691 span is unlikely, and the presence of the marine levels found in the northeastern Cameros Basin (Enciso
692 Group) can be satisfactory explained as exclusively related to northern marine incursions (Fig. 17B).

693 **9.3. Middle Albian palaeogeography**

694 The middle-late Albian successions of the Escucha Fm recorded in the Bigornia trough indicates the

695 episodic setting of coastal marine sedimentary domains (with oysters, echinoderms and serpulids) in the
696 southeastern marginal areas of the Cameros Basin. The coeval successions of Grávalos, located in the
697 footwall of the North Cameros thrust (Fig. 17C), include more open marine intervals, with abundant
698 rudists. According to Muñoz et al. (1997), there is a gradual transition between these shallow marine
699 facies and the coal-rich transitional successions typical of the Escucha Fm.

700 Following Clemente (2010), the equivalent unit to the Escucha Fm in the western Cameros Basin is the
701 upper part of the Salas Group, a largely progradational fluvial system with evidence of aeolian facies,
702 unconformably overlain by the postrift sandstones of the Utrillas Fm. Terrigenous input of this fluvial
703 system was sourced from the western uplifted Iberian Massif, and drained the basin towards the north-
704 northeast, passing gradually to a tide-influenced coastal plain. According to Clemente (2010), the middle-
705 upper part of the Salas Group in the Soria-Abejar area includes relatively thick intervals of facies with
706 inclined heterolithic strata and coal of possibly tidal origin. Marine incursions in the eastern Cameros
707 Basin were sourced from the north (Muñoz *et al.*, 1997; Clemente, 2010). An alternative source from the
708 southeastern Tethysian domain is unlikely, since the coastal marine sedimentation during the Albian in
709 the Maestrazgo Basin was confined south to the Oliete Subbasin, in its eastern depocentral areas (Fig.
710 17C; Querol et al., 1992; García et al., 2004; Liesa et al., 2019).

711

712 **10. CONCLUSIONS**

713 The review of the stratigraphy, sedimentology, structural evolution and vertebrate fossil record of the
714 synrift deposits of the Torrelapaja Subbasin (southeastern Cameros Basin) presented in this study has
715 provided the following main findings:

716 1- The evolution of the uppermost Jurassic-Lower Cretaceous Torrelapaja Subbasin was mostly
717 controlled by the activity of the three major NW-SE trending extensional faults: Malanquilla Fault

718 (southwest-dipping), Berdejo Fault (northeast-dipping) and Carabantes Fault System (northeast-dipping).
719 The subbasin was longitudinally subdivided into the Bigornia and Bijuesca troughs by the Berdejo Fault.
720 The Bigornia trough is located very close to the South Cameros Fault and it recorded the most complete
721 and thicker synrift sedimentary succession.

722 2- Discontinuous activity of the major NW-SE trending faults combined to other minor faults with
723 variable orientation (around NE-SW trending) resulted in an irregular uppermost Jurassic-Lower
724 Cretaceous sedimentary record. The complex geometry of the Torrelapaja Subbasin reconstructed in this
725 work is defined by this two nearly perpendicular fault sets acting simultaneously. The greater significance
726 of faults in NW-SE suggests a direction of main NE-SW extension and a secondary NW-SE extension, as
727 has also been previously proposed for the Cameros Basin.

728 3- The sedimentary record of the Torrelapaja Subbasin consist of three synrift sequences (SS-1, SS-2 and
729 SS-3) bounded by major unconformities. These unconformities are related to the reactivation of
730 different sets of faults during the different stages of evolution of the subbasin. The Tithonian–middle
731 Berriasian SS-1 (Bijuesca and Ciria formations) occurs across the entire Torrelapaja Subbasin, whereas
732 the uppermost Hauterivian–lower Barremian SS-2 (Torrelapaja Fm) and the middle–upper Albian SS-3
733 (Escucha Fm) are recorded with significant thickness only in the northern part of the subbasin, in the
734 Bigornia trough.

735 4- The large sedimentary record of SS-1 occurs in the Bijuesca trough (up to 220 m) and in the
736 northwestern Bigornia trough, where the presence of NE-SW trending faults involved the presence of
737 highly subsident blocks, with up to 350–400 m-thick deposits. Sedimentation of SS-1 occurred in alluvial
738 fan systems, sourced from the uplifted basin margins, exposing the marine Jurassic carbonate rocks. The
739 progressive degradation of the relief favoured the expansion of the carbonate palustrine to lacustrine
740 environments across the entire sedimentation areas during the early-middle Berriasian. The new
741 discovered vertebrate fossil site of La Atalaya (Bijuesca trough) includes large sized sauropods and

742 crocodylomorphs preserved in palustrine facies, and was most probably formed around the Tithonian-
743 Berriasian transition.

744 5- The boundary between SS-1 and SS-2 is a widespread unconformity associated to an upper Berriasian-
745 lower Hauterivian stratigraphic gap. The thickest record of SS-2 (Torrelapaja Fm) found in the
746 southeastern part of the Bigornia trough (up to 80 m) was mostly controlled by the activity of the
747 Malanquilla and Berdejo NW-SE trending faults, combined to a set of small-scale faults with variable
748 orientations around NW-SE. A locally deep-incised palaeokarst developed on top of the Berriasian
749 lacustrine carbonates was filled by a few dm-thick multiphase levels of muddy distal alluvial facies
750 around the Hauterivian-Barremian transition. These facies include the new discovered vertebrate fossil
751 sites of Corrales de las Cañadas, Corrales de Valdelavieja and Valdelatorre, with a dinosaur-dominated
752 macrovertebrate record of sauropod, theropod and ornithopod remains. After this stage of condensed
753 and irregular sedimentation, a second early Barremian stage of muddy distal alluvial plains with
754 paleosoils and Fe-pisoids as well as palustrine-shallow lacustrine carbonate systems developed. At the
755 third stage, increased tectonic activity involved larger terrigenous-clastic input sourced from the
756 southeast, and the development of middle-distal alluvial systems, and distal mud flats with small
757 carbonate ponds in the central part of the Bigornia trough.

758 6- The SS-3 (Escucha Fm) includes shales and intercalated sandy-skeletal limestones with abundant
759 oysters and plant debris. This unit is assigned here to the middle-upper Albian based in regional
760 correlation and strontium isotopic data. The widespread presence of oysters and other marine skeletal
761 debris (serpulids, echinoderms) indicates the first marine incursion in the studied basin, with marine
762 waters sourced from the north (Bay of Biscay domain). The overall palaeogeography of the Iberian Basin
763 rift system during the Early Cretaceous reviewed and updated here makes unlikely an alternative marine
764 source from the southeast (Tethysian realm) as suggested in previous works. Accordingly, the results
765 presented here might have further implications for the understanding of the overall evolution of the

766 latest Jurassic-Early Cretaceous Iberian rifting, as clarifying the distribution in time and space of
767 Thetysian and northern affinities of the different paleogeographical domains, and the causes and
768 processes laying behind.

769

770 **Acknowledgments**

771 This study was subsidized by the Spanish Ministerio de Economía y Competitividad-ERDF (Project
772 CGL2017-85038-P), the Spanish State Research Agency (Project PID2019-108705GB-I00), as well as by
773 the Aragón Regional Government and the European Regional Development Fund (research groups
774 E18_20R *Aragosaurus: recursos geológicos y paleoambientes* and E32_20R *Geotransfer: investigación*
775 *geológica para la ciencia y la sociedad*). We thank Prof. Carles Martín-Closas for the assistance in the
776 charophyte determination. We also acknowledge the suggestions provided by the two reviewers
777 (professors Marian Fregenal-Martínez and Bruno Granier) that helped to improve the quality of the
778 original manuscript. We also appreciate the technical assistance of the *Servicio General de Apoyo a la*
779 *Investigación-SAI*, Universidad de Zaragoza. DC is supported by the *Beatriu de Pinós* postdoctoral
780 programme (BP2017-00195) of the Government of Catalonia's Secretariat for Universities and Research
781 of the Ministry of Economy and Knowledge.

782

783 **REFERENCES**

- 784 Allix, P., Burnham, A., Fowler, T., Herron, M., Kleinberg, R., Symington, B. (2011): Coaxing oil from Shale.
785 *Oilfield Review* 22 (4), 4–15.
- 786 Alonso, A., Mas, J. R. (1988): La transgresión Aptiense al sur del Moncayo (límite de las provincias de
787 Soria y Zaragoza). *II Congreso geológico de España Vol 1*, Granada: p. 11–15.

- 788 Alonso, A., Mas, J.R. (1990): El Jurásico Superior marino en el sector Demanda- Cameros (La Rioja-Soria).
789 *Cuadernos de Geología Ibérica*, 14, 173–198.
- 790 Alonso, A., Mas, J. R. (1993): Control tectónico e influencia del eustatismo en la sedimentación del
791 Cretácico inferior de la cuenca de Los Cameros. *Cuadernos de Geología Ibérica* 17, 285–310.
- 792 Alonso, A., Floquet, M., Mas, R., Meléndez, A. (1993): Late Cretaceous Platforms: Origin and evolution,
793 Iberian Range, Spain. In: J. A. Toni Simo, R. W. Scott, J. P. Masse (eds.), *Cretaceous Carbonate*
794 *Platforms*, AAPG Memoir 56: 297–313.
- 795 Antolín-Tomás, B., Liesa, C.L., Casas, A.M., Gil-Peña, I. (2007). Geometry of fracturing linked to extension
796 and basin formation in the Maestrazgo basin (Eastern Iberian Chain, Spain). *Revista de la Sociedad*
797 *Geológica de España*, 20, 351-365.
- 798 Aurell, M., Bádenas, B., Gasca, J.M., Canudo, J.I., Liesa, C., Soria, A.R., Moreno-Azanza, M., Najes, L.
799 (2016): Stratigraphy and evolution of the Galve sub-basin (Spain) in the middle Tithonian-early
800 Barremian: implications for the setting and age of some dinosaur fossil sites. *Cretaceous Research* 65,
801 138–162.
- 802 Aurell, M., Soria, A.R., Bádenas, B., Liesa, C.L., Canudo, J.I., Gasca, J.M., Moreno-Azanza, M., Medrano-
803 Aguado, E., Meléndez, A. (2018): Barremian synrift sedimentation in the Oliete sub-basin (Iberian
804 Basin, Spain): palaeogeographical evolution and distribution of vertebrate remains. *Journal of Iberian*
805 *Geology*, 44, 285–308.
- 806 Aurell, M., Bádenas, B., Canudo, J.I., Castanera, D., García-Penas, A., Gasca, J.M., Martín-Closas, C.,
807 Moliner, L., Moreno-Azanza, M., Rosales, I., Santas, L., Sequero, C., Val, J. (2019a): Kimmeridgian–
808 Berriasian stratigraphy and sedimentary evolution of the central Iberian Rift System (NE Spain).
809 *Cretaceous Research* 102, 1–19.

- 810 Aurell, M., Fregenal-Martínez, M., Bádenas, B., Muñoz-García, M.B., Élez, J., Meléndez, N., de
811 Santisteban, C. (2019b): Middle Jurassic–Early Cretaceous tectono-sedimentary evolution of the
812 southwestern Iberian Basin (central Spain): Major palaeogeographical changes in the geotectonic
813 framework of the Western Tethys. *Earth Science Reviews* 199, 102983.
- 814 Bádenas, B., Aurell, M. (2001): Kimmeridgian palaeogeography and basin evolution of northeastern
815 Iberia. *Palaeogeography, Palaeoclimatology, Palaeoecology* 168, 291–310.
- 816 Bádenas, B., Salas, R. and Aurell, M. (2004): Three orders of regional sea-level changes control facies and
817 stacking patterns of shallow carbonates in the Maestrat Basin (Tithonian–Berriasian, NE Spain).
818 *International Journal of Earth Sciences*, 93, 144–162.
- 819 Bádenas, B., Aurell, M., Gasca, J.M. (2018): Facies model of a mixed clastic-carbonate, wave-dominated
820 open-coast tidal flat (Tithonian-Berriasian, north-east Spain). *Sedimentology* 65, 1631–1666.
- 821 Bralower, T. J., Fullagar, P. D., Paull, C. K., Dwyer, G. S., & Leckie, R. M. (1997). Mid-Cretaceous strontium-
822 isotope stratigraphy of deep-sea sections. *Geological Society of America Bulletin*, 109, 1421–1442.
- 823 Bryant, J. D., Jones, D. S., & Mueller, P. A. (1995). Influence of fresh-water flux on $^{87}\text{Sr}/^{86}\text{Sr}$
824 chronostratigraphy in marginal marine environments and dating of vertebrate and invertebrate
825 faunas. *Journal of Paleontology*, 69, 1–6.
- 826 Canérot J (1974): Recherches géologiques aux confins des Chaînes ibériques et catalane (Espagne). Ph.D.
827 Thesis. Sc. Nat. Toulouse, ENADISMA, Trabajos de tesis.
- 828 Canudo J.I., Barco J.L., Castanera D., Torcida-Baldor F. (2010): New record of an enigmatic sauropod in
829 the Jurassic-Cretaceous transition of the Iberian Peninsula (Spain). *Paläontologische Zeitschrift* 84,
830 427–435.
- 831 Capote, R., Muñoz, J.A., Simón, J.L., Liesa, L.C., Arlegui, L.E. (2002) Alpine tectonics I: the alpine system

- 832 north of the Betic Cordillera. In: The Geology of Spain (Eds. by W. Gibbons & T. Moreno), The
833 Geological Society, London. pp. 367-400.
- 834 Casas, A.M., Villalaín, J.J., Soto, R., Gil-Imaz, A., del Río, P., Fernández, G. (2009): Multidisciplinary
835 approach to an extensional syncline model for the Mesozoic Cameros Basin (N Spain). *Tectonophysics*
836 470, 3–20.
- 837 Clemente, P. (2010): Review of the Upper Jurassic-Lower Cretaceous Stratigraphy in Western Cameros
838 basin, Northern Spain. *Revista de la Sociedad Geológica de España* 23 (3-4), 101–143.
- 839 Colombo, F. (1994): Normal and reverse unroofing sequences in syntectonic conglomerates as evidence
840 of progressive basinward deformation. *Geology* 22 (3): 235–238
- 841 Cortés, A.L., Liesa, C.L., Soria, A.R., Meléndez, A. (1999). Role of extensional structures on the location of
842 folds and thrusts during tectonic inversion (Northern Iberian Chain, Spain). *Geodinamica Acta*, 12(2),
843 113–132.
- 844 Denison, R.E. Miller, N.R. Scott, R.W., Reaser D.F. (2003): Strontium isotope stratigraphy of the
845 Comanchean Series in north Texas and southern Oklahoma. *Geological Society of America Bulletin*
846 115, 669–682
- 847 Fuentes-Vidarte, C., Mejjide-Calvo, M., Mejjide-Fuentes, F., Mejjide-Fuentes, M. (2016): Un nuevo
848 dinosaurio estiracosterno (Ornithopoda: Ankylopollexia) del Cretácico Inferior de España. *Spanish*
849 *Journal of Palaeontology*, 31 (2), 407–446.
- 850 García A. (coord.) (1982): Recapitulación: In: *El Cretácico de España*. Univ. Complutense Madrid, 655–
851 680.
- 852 García, A. Mas, R., Segura, M., Carenas, B., García-Hidalgo, J. F., Gil, J., Alonso, A., Aurell, M., Bádenas, B.,
853 Benito, M. I., Meléndez, A., Salas, R. (2004): Segunda fase de postrift: Cretacico Superior. In: J. A.

- 854 Vera, *Geología de España*. Sociedad Geológica de España-Instituto Geológico y Minero, Madrid: 510–
855 522.
- 856 García-Lasanta, C., Oliva-Urcia, B., Román-Berdiel, T., Casas, A.M., Hirt, A.M. (2014). Understanding the
857 Mesozoic kinematic evolution in the Cameros basin (Iberian Range, NE, Spain). *Journal of Structural*
858 *Geology*, 66: 84-101.
- 859 García-Mondéjar, J. (1990): The Aptian-Albian carbonate episode of the Basque-Cantabrian Basin
860 (northern Spain): general characteristics, controls and evolution. In: *Carbonate Platforms: Facies,*
861 *Sequences and Evolution* (M.E. Tucker, J.L. Wilson, P.D. Crevello, J.F. Sargy J.F. Read, Eds.), Blackwell,
862 Int. Assoc. Sedimentologists Special Publication 9, 257–290
- 863 Gasca, J. M., Moreno-Azanza, M., Bádenas, B., Díaz-Martínez, I., Castanera, D., Canudo, J. I., & Aurell, M.
864 (2017): Integrated overview of the vertebrate fossil record of the Ladruñán anticline (Spain): evidence
865 of a Barremian alluvial-lacustrine system in NE Iberia frequented by dinosaurs. *Palaeogeography,*
866 *Palaeoclimatology, Palaeoecology*, 472, 192–202.
- 867 Gómez-Fernández, J.C. and Meléndez, N. (1994): Estratigrafía de la Cuenca de los Cameros (Cordillera
868 Ibérica Noroccidental, N de España) durante el tránsito Jurásico-Cretácico. *Revista de la Sociedad*
869 *Geológica de España*, 7, 121–39.
- 870 Guimerà, J., Mas, R., Alonso, A. (2004): Intraplate deformation in the NW Iberian Chain: Mesozoic
871 extension and Tertiary contractional inversion. *Journal of the Geological Society, London*. (161), 291–
872 303.
- 873 Guiraud, M., Séguret, M. (1984). Releasing solitary overstep model for the Late Jurassic-Early Cretaceous
874 (Wealdian) Soria strike-slip basin (North Spain). In: *Strike slip deformation, basin formation and*
875 *sedimentation* (K.T. Biddle and N. Christie-Blick, eds.). SEPM Spec. Publ. 37, 159-175.
- 876 Hernández-Medrano, N., Pascual Arribas, C. P., Latorre Macarrón, P., Sanz Pérez, E. (2005). Contribución

- 877 de los yacimientos de icnitas sorianos al registro general de Cameros. *Zubía*, (23), 79–120.
- 878 IGME (1984): Exploración de lignitos en las áreas de Casarejos (Soria), Contreras (Burgos), Reznos (Soria),
879 Embid de Ariza-Almazul (Soria-Zaragoza) y Bijuesca-Torrelapaja (Soria-Zaragoza). Instituto Geológico y
880 Minero de España, Ministerio de Industria y Energía, Madrid, 1–120.
- 881 Isasmendi, E., Sáez-Benito, P., Torices, A., Navarro-Lorbés, P., Pereda-Suberbiola, X. (2020). New insights
882 about theropod palaeobiodiversity in the Iberian Peninsula and Europe: Spinosaurid teeth
883 (Theropoda, Megalosauroidea) from the Lower Cretaceous of La Rioja (Spain). *Cretaceous Research*,
884 116, 104600.
- 885 Laita, E., Bauluz, B, Aurell, M., Bádenas, B., Canudo, J.I., Yuste, A. (2020). A change from warm/humid to
886 cold/dry climate conditions recorded in lower Barremian clay-dominated continental successions
887 from the SE Iberian Chain (NE Spain). *Sedimentary Geology* 403 (2020) 105673
- 888 Liesa, C.L., Casas, A.M., Simón, J.L. (2018). La tectónica de inversión en una región intraplaca: La
889 Cordillera Ibérica. *Revista de la Sociedad Geológica de España*, 31: 23-50.
- 890 Liesa, C.L., Soria, A.R., Casas, A., Aurell, M., Meléndez, N., Bádenas, B., Fregenal-Martínez, M., Navarrete,
891 R., Peropadre, C., Rodríguez-López, J.P. (2019): The South Iberian, Central-Iberian and Maestrazgo
892 basins. In: Quesada, C., Oliveira, J.T. (Eds.), *The Geology of Iberia: A Geodynamic Approach* Vol. 5.
893 Springer Nature Switzerland AG, Alpine Cycle, pp. 214–228.
- 894 Liesa, C.L., Soria, A.R., Meléndez, N., Meléndez, A. (2006). Extensional fault control on the sedimentation
895 patterns in a continental rift basin: El Castellar Formation, Galve subbasin, Spain. *Journal of the*
896 *Geological Society of London*, 163, 487–498.
- 897 Marqués, L., Maestro, A., Gil, A., Casas, A..M. (1996). Aportaciones del análisis microestructural a la
898 evolución tectónica del extremo oriental de la Cuenca de Cameros. *Geogaceta* 20(4), 767-769.

- 899 Martín-Closas, C. (1989): Els caròfits del Cretaci Inferior de les conques perifèriques del Bloc de l'Ebre.
900 PhD thesis. University of Barcelona.
- 901 Mas, R., Alonso, A., Guimerà, J. (1993). Evolución tectonosedimentaria de una cuenca extensional
902 intraplaca: La cuenca finijurásica-eocretácica de Los Cameros (La Rioja-Soria). *Revista de la Sociedad*
903 *Geológica de España*, 6: 129-144.
- 904 Mas, R., Benito, M. I., Arribas, J., Serrano, A., Guimerà, J., Alonso, A., Alonso-Azcárate, J. (2002): La
905 Cuenca de Cameros: desde la extensión finijurásica-eocretácica a la inversión terciaria – implicaciones
906 en la exploración de hidrocarburos. *Zubía Monográfico* 14, 9–64.
- 907 Mas, R., García, A., Salas, R., Meléndez, A., Alonso, A., Aurell, M., Bádenas, B., Benito, M. I., Carenas, B.,
908 García-Hidalgo, J. F., Gil, J., Segura, M. (2004): Segunda Fase de rifting: Jurásico Superior-Cretácico
909 Inferior. In: J. A. Vera, *Geología de España*. Sociedad Geológica de España-Instituto Geológico y
910 Minero, Madrid: 503–510.
- 911 Mas, R., Benito, M.I., Arribas, J., Omodeo-Salé, S., Suarez-Gonzalez, P., Quijada, I.E., Guimerà, J.,
912 González-Acebrón, L., Arribas, M.E. (2019): The Cameros Basin. In: Quesada, C., Oliveira, J.T. (Eds.),
913 *The Geology of Iberia: A Geodynamic Approach* Vol. 5. Springer Nature Switzerland AG, Alpine Cycle,
914 pp. 190–205.
- 915 McArthur, J.M., Howarth, R.J., Shields, G.A. (2012). Strontium isotope stratigraphy. In F. M. Gradstein, J.
916 G. Ogg, M. D. Schmitz, & G. M. Ogg (Eds.), *The Geological Time Scale 2012* (pp. 127–144). Oxford:
917 Elsevier B.V.
- 918 Meléndez, N., Liesa, C.L., Soria, A.R., Meléndez, A. (2009). Lacustrine evolution during early rifting: El
919 Castellar Formation (Galve sub-basin, Central Iberian Chain). *Sedimentary Geology* 222, 64-77.
- 920 Moratalla, J.J., Hernán, J. (2010): Probable palaeogeographic influences of the Lower Cretaceous Iberian

- 921 rifting phase in the Eastern Cameros Basin (Spain) on dinosaur trackway orientations.
- 922 *Palaeogeography, Palaeoclimatology, Palaeoecology* 295, 116–130
- 923 Moreno-Azanza, M., Gasca, J.M., Díaz-Martínez, I., Bauluz Lázaro, B., Canudo Sanagustín, J.I., Fernández,
924 A., Pérez- Lorente, F. (2016): A multi-ootaxic assemblage from the Lower Cretaceous of the Cameros
925 Basin (La Rioja; Northern Spain). *Spanish Journal of Palaeontology*, 31 (2), 305–320.
- 926 Muñoz, A., Soria, A., Canudo, J. I., Casas, A. M., Gil, A., Mata, M. P. (1997): Caracterización estratigráfica y
927 sedimentológica del Albiense marino del borde Norte de la Sierra de Cameros. Implicaciones
928 Paleogeográficas. *Cuadernos de Geología Ibérica* 22, 139–163
- 929 Muñoz, A., Angulo, A., Liesa, C.L., Luzón, M.A., Mayayo, M.J., Pérez, A., Soria, A.R., Val, V., Yuste, A.
930 (2020). Periodicidad climática y datación astrocronológica del Grupo Enciso en la Cuenca oriental de
931 Cameros (N de España). *Boletín Geológico y Minero*, 131, 2, doi. 10.21701/bolgeomin.131.2.003.
- 932 Navarro-Vázquez, D. (coord) (1991): Mapa Geológico de España, 1:50000. Num 380 (Borobia). Instituto
933 Tecnológico Geominero de España, Madrid.
- 934 Pérez-Lorente, F. (2015). *Dinosaur footprints and trackways of La Rioja*. Indiana University Press.
- 935 Platt, N.H. (1990). Basin evolution and fault reactivation in the Western Cameros Basin, Northern Spain.
936 *Journal of the Geological Society of London* 147, 165-175.
- 937 Pujalte, V., Robles, S., García-Ramos, J.C., Hernández, J.M. (2004): El Malm-Barremiense no marino de la
938 Cordillera Cantábrica. In: J. A. Vera, *Geología de España*. Sociedad Geológica de España-Instituto
939 Geológico y Minero, Madrid: 288–291.
- 940 Querol, X., Salas, R., Pardo, G., Ardevol, L. (1992): Albian coal-bearing deposits of the Iberian Range in
941 northeastern Spain. In: McCabe, J.P., Panish, J.T. (Eds.), Controls and distribution and quality of
942 Cretaceous coals. *Geological Society of America, Special Paper* 267, 193–208.

- 943 Quijada, I.E., Suarez-Gonzalez, P., Benito, M.I., Mas, J.R. (2013): New insights on the stratigraphy and
944 sedimentology of the Oncala Group (eastern Cameros Basin): implications for the paleogeographic
945 reconstruction of NE Iberia at Berriasian times. *Journal of Iberian Geology* 39, 313–334.
- 946 Quijada, I.E., Benito, M.I., Suarez-Gonzalez, P., Rodriguez-Martínez, M., Campos-Soto, S. (2020):
947 Challenges to carbonate-evaporite peritidal facies models and cycles: Insights from Lower Cretaceous
948 stromatolite-bearing deposits (Oncala Group, N Spain). *Sedimentary Geology*, 408 105752
- 949 Rey-Martínez, G, Royo-Torres, R. (2014): Estudio paleontológico de una tibia de dinosaurio saurópodo de
950 la Formación Ciria (Titoniense–Berriasiense) hallada en Berdejo (Zaragoza). *XII Encuentro de Jóvenes*
951 *Investigadores en Paleontología (Boltaña, 2014)*. 105–108.
- 952 Royo-Torres, R., Gascó, F., Cobos, A. (2012): Dinosaurs from Zaragoza province (Iberian Range, Spain).
953 *Fundamental*, 20, 215–218.
- 954 Sacristán-Horrajada, S., Eugenia Arribas, M., Más, R. (2011): Sedimentología de sucesiones sinrift
955 tempranas en un semigraben marginal de un rift extensional: la Cuenca de Bijuesca, Jurásico superior
956 de la Cordillera Ibérica (Zaragoza, España). *Geogaceta*, 50-2: 121–124.
- 957 Sacristán-Horrajada, S., Carrasco, A., Mas, R., Arribas, M.E. (2012): Comparación del registro
958 estratigráfico de dos cubetas satélites asociadas a un sistema de *rift*: los surcos de Bijuesca y
959 Bigornia (SE de la Cuenca de Cameros). *Geo-Temas* 13 (2): 155-158 (02_108-111 in CD).
- 960 Salas, R., Guimerà, J., Mas, R., Martín-Closas, C., Meléndez, A., Alonso, A. (2001): Evolution of the
961 Mesozoic Central Iberian Rift System and its Cainozoic inversion (Iberian chain). In: P.A. Ziegler, W.
962 Cavazza, A.H.F. Robertson, S. Crasquin-Soleau (eds.), *Peri-Tethys Memoir 6: Peri-Tethyan rift/wrench*
963 *basins and passive margins*. Mémoires du Musée nat. Hist. naturelles de Paris 186, 145–185.
- 964 Salomon, J. (1982): Cameros-Castilla: El Cretácico Inferior. In A. García (Ed.), *El Cretácico de España* (pp.

- 965 345–387). Madrid: Univ. Complutense de Madrid.
- 966 San Román, J., Aurell, M. (1992): Palaeogeographical significance of the Triassic–Jurassic unconformity in
967 the north Iberian basin (Sierra del Moncayo, Spain). *Palaeogeography, Palaeoclimatology,*
968 *Palaeoecology*, 99, 101–117.
- 969 Schudack, M. (1987): Charophyten flora und fazielle Entwicklung der Grenzsichten mariner Jura-
970 Wealden in den Nordwestlichen Iberischen Ketten (mit Vergleichen zu Asturien und Kantabrien).
971 *Palaeontographica Abteilung B* 204, 1–180.
- 972 Schudack, U., Schudack, M. (2009): Ostracod biostratigraphy in the Lower Cretaceous of the Iberian
973 chain (Eastern Spain). *Journal of Iberian Geology* 35, 141–168.
- 974 Soria, A.R., Martín-Closas, C., Meléndez, A., Meléndez, N., Aurell, M. (1995): Estratigrafía del Cretácico
975 Inferior del sector central de la Cordillera Ibérica. *Estudios Geológicos* 51, 141–152.
- 976 Suárez-González P, Quijada IE, Benito MI, Mas R (2013): Eustatic versus tectonic control in an intraplate
977 rift basin (Leza Fm, Cameros Basin): chronostratigraphic and paleogeographic implications for the
978 Aptian of Iberia. *Journal of Iberian Geology* 39: 285–312.
- 979 Torcida Fernández-Baldor, F., Canudo, J.I., Huerta, P., Moreno-Azanza, M., Montero, D. (2017):
980 *Europatitan eastwoodi*, a new sauropod from the Lower Cretaceous of Iberia in the initial radiation of
981 somphospondylians in Laurasia. *PeerJ*, 5:e3409.

982 **FIGURE CAPTIONS**

983 Fig. 1. - (A) Geological location of the Torrelapaja Subbasin. The map of the Iberian Peninsula shows the
984 distribution of Mesozoic outcrops and the location of three main uppermost Jurassic-Lower Cretaceous
985 sedimentary domains of Northeast Iberia: Maestrazgo (Ma), Cameros (Ca) and Basque-Cantabrian (BC)
986 basins; (B) Geological restored section at the end of Mesozoic extension through the eastern part of the
987 Cameros Basin (see dashed line in A for location). Modified from Guimerà et al. (2004), with
988 reconstruction of the Torrelapaja Subbasin based on data exposed in this work.

989 Fig. 2. - Summary of the stratigraphy of the Torrelapaja Subbasin. Major discontinuities D1–D5 separate
990 the successive synrift and postrift Mesozoic sequences. Abbreviated names of units of right column refer
991 to those used in the geological mapping of Figure 4. The studied synrift sequences (SS) shadowed in gray
992 in the central column are very variable in thickness.

993 Fig. 3. - Geological mapping of the area including the Torrelapaja Subbasin. The mapping of the squared
994 areas A, B and C is enlarged in Figure 4.

995 Fig. 4. – Detailed geological mapping of some key areas (see Figs. 2 and 3 for legend of stratigraphic units
996 and location). (A) Northern area: the orange stars locate in the abandoned coal mines in the upper
997 Escucha Fm; the two green stars indicates the sampling points for charophytes of Martín-Closas (1989) in
998 the Ciria and Torrelapaja formations respectively; (B) Central area: the black arrows indicate the location
999 of La Cañada (LC), Valdelatorre (VT) and Valdelavieja (VJ) logs in the Torrelapaja Fm; the red squares
1000 indicate the new fossil sites of Corrales de Las Cañadas (CC), Valdelatorre (VT) and Corrales de
1001 Valdelavieja (CV); the pink squares correspond to the fossil sites BJ1 and BJ5 of Royo-Torres et al. (2012),
1002 the red squares indicate the new dinosaur fossil sites of Corrales de Las Cañadas (LC), Valdelatorre (VT),
1003 Valdelavieja (VJ) in the Torrelapaja Fm (see Fig. 10 for their stratigraphic location); the green star in B is
1004 the sampling point for the *Exogyra* shells used in the strontium analysis of the Escucha Fm; (C) Southern
1005 area with location of the Bijuesca (BJ) log and the new discovered fossil site of La Atalaya (LA) in the

1006 Bijuesca Fm (see red square).

1007 Fig. 5. - The synrift sequence 1 in the Bijuesca trough. (A) General view of the Bijuesca outcrop, showing
1008 the distribution of units. The left part shows the angular unconformity with the Utrillas Fm. The yellow
1009 star locates the La Atalaya fossil site in the topmost levels of the Bijuesca Fm; (B) Fining-upward
1010 sequence in the upper Bijuesca Fm, ending with nodular/brecciated limestones with root traces. The
1011 yellow star indicates the carbonate level including La Atalaya fossil site (see Fig. 10 for its stratigraphic
1012 location); (C) Detail of the paraconformity between the lower Kimmeridgian reef limestones of the
1013 Torrecilla Fm and the conglomerates, sandstones and mudstones of the Bijuesca Fm; (D) Large-sized limb
1014 bone fragment assigned to Sauropoda indet floating in a nodular/brecciated limestones in La Atalaya
1015 site; (E) Large-sized caudal vertebra assigned to Sauropoda indet. encased in burrowed marls in La
1016 Atalaya site; (F) A fining-upward sequence from conglomerates to sandstones to red mudstones in the
1017 upper Bijuesca Fm; (G) Close view of clast-supported conglomerates with poorly rounded Jurassic
1018 limestone clasts with normal gradation in the middle part of the Bijuesca Fm.

1019 Fig. 6. - The synrift sequence 2 in the outcrops located around Valdelavieja-Valdelatorre logs. (A) Highly
1020 irregular paleokarst developed on top of the Ciria Fm in Valdelavieja log, including the fossil site of CV.
1021 The overlying level (white star) includes the samples CV-2 and CV-3 (see fig. 10); (B) The infill of the karst
1022 cavities in Valdelavieja has yield two theropod? vertebrae (see white arrows) and other remains; (C)
1023 Rippled sandstones in the middle part of the Torrelapaja Fm; (D) General view of the outcrop of
1024 Valdelatorre exposing the ochre marlstones/calcareous mudstones of the lower part of the Torrelapaja
1025 Fm. The yellow star indicates the location of the Berdejo-1 (BJ-1) fossil site of Royo-Torres et al. (2012);
1026 (E) Close view of the grain-supported conglomerates with quartzite clasts and normal gradation found in
1027 the middle part of the Torrelapaja Fm in the Valdelavieja log; (F) Close view of the tufa level with
1028 abundant debris of coated plant stems exposed in the upper part of the Torrelapaja Fm in the
1029 Valdelatorre log.

1030 Fig. 7. - Field views of Las Cañadas log. (A) Large karst cavity developed on top of the Ciria Fm filled by
1031 reddish mudstones; (B) Close view of the sauropod humerus recovered in the paleokarstic cavity of Las
1032 Cañadas; (C) General view of the outcrop of Las Cañadas; (D) Red mudstones with hydromorphic soils of
1033 the upper part of the Torrelapaja Fm in Las Cañadas log; (E) Boundary between SS-2 (Torrelapaja Fm) and
1034 SS-3 (Escucha Fm) in Las Cañadas outcrop; (F) Sandy skeletal limestone rich in oyster shells typical of the
1035 lower part of the Escucha Fm.

1036 Fig. 8. – Oblique aerial view (above) and outcrop image (below) of two examples showing the angular
1037 unconformity between SS-1 (Ciria Fm) and SS-2 (Torrelapaja Fm) in the southeastern part of the Bigornia
1038 trough. The example of the right includes the Corrales de Las Cañadas fossil site. Note as the angular
1039 unconformity fossilizes decametric-scale normal faults affecting the Ciria Fm limestones, and the lower
1040 Torrelapaja Fm beds onlap the unconformity.

1041 Fig. 9. - Sedimentological features of the Bijuesca and Ciria formations. (A) Stratigraphic log indicating
1042 the facies distribution of the Bijuesca and Ciria formations in Bijuesca locality (redrawn and slightly
1043 modified from Sacristan-Horcajada et al., 2011; see BJ in Fig. 4C for location), and the location of La
1044 Atalaya fossil site; (B) Stratigraphic log indicating the facies distribution of the Ciria Fm in Las Cañadas 1
1045 log (LC1; see Fig. 4B for location); (C-D) Thin section images in plane-polarized light of limestone facies of
1046 the Ciria Fm: (C) palustrine limestones with charophytes and fenestral porosity (see 1); and (D) oncolitic
1047 limestones with cm-thick oncoids with charophytes in the nuclei (see 1).

1048 Fig. 10. - Sedimentological features of the Torrelapaja Fm. (A) Stratigraphic logs indicating the facies
1049 distribution of the Torrelapaja Fm (see Fig. 4B for location). The three sedimentary stages differentiated
1050 and the location of the fossil sites of Corrales de Valdelavieja (CJ), Valdelatorre (VT), Corrales de Las
1051 Cañadas (CC) and Berdejo-1 (BJ-1) are also indicated; (B) Mineralogical composition of muddy facies of
1052 the unit (tertiary diagram adapted from Allix et al., 2011).

1053 Fig. 11. Thin sections images in plane-polarized light of limestone facies of the Torrelapaja Fm. (A)

1054 Intraclastic/litoclastic facies with quartz sand and quartzite lithoclasts (Paleozoic: see 1), limestone
1055 (Jurassic) lithoclasts (see echinoid spine in 2 and ooids in 3), intraclasts of bioclastic facies (see 4), oncid
1056 fragments (see 5) and vertebrate remains (see 6); (B–D) Lacustrine bioclastic limestones, including (B)
1057 bivalve and gastropod packstone and (C) bioturbated ostracod wackestone/packstone, with
1058 accumulation of skeletal debris produced by hydrodynamic sorting; and (D) ostracod and charophyte
1059 wackestone; (E) Fenestral bioclastic limestone with ostracods and charophytes formed in palustrine
1060 areas. Notice fenestral porosity (see 1), charophytes (see 2) and oncid fragments (see 3); (F–G) Tufa
1061 limestones including (F) oncolitic packstones/grainstones with entire and broken oncoids, with bioclastic
1062 and intraclastic cores and cortices formed by sub-mm to mm alternation dark micritic laminae (see 1),
1063 and porous micritic laminae with microbial filaments perpendicular to laminae (see 2), intraclasts of
1064 stromatolites (see 3) and coated plant stems (see 4); and (G) phytoclastic packstones big clasts of coated
1065 plant stems and stromatolites, in an packstone matrix of smaller intraclasts and oncid fragments.

1066 Fig. 12. Palaeoenvironmental reconstruction of facies of sedimentary stages 1 to 3 of the Torrelapaja Fm
1067 (see Fig. 10 for legend of facies).

1068 Fig. 13. (A) Sedimentological features of the Escucha Fm (SS-3) in the Valdelavieja 3 log (see VJ3 in Fig. 4B
1069 for location); (B–C) Thin sections images in plane-polarized light of limestone facies, including (B) sandy
1070 bioclastic limestones, with abundant oysters and gastropods, intraclasts of muddy limestones (see 1)
1071 and sandstones (see 2) and carbonaceous material (see 3); and (C) bivalve sandy limestones, with
1072 accumulated debris of oysters, and some serpulids (see 1) and carbonaceous material (see 2). (D)
1073 Strontium isotopic curve of McArthur et al. (2012) during Barremian–Albian (in light gray) indicating the
1074 interval comprising the three values obtained from the Escucha Fm (with diamonds, left part).
1075 Considering the time constrains provided by the Torrelapaja and Utrillas formations, the obtained
1076 isotopic values are compatible with two time intervals (see dark grey surface). However, regional data
1077 and overall palaeogeography of northeast Iberian clearly point to a middle-late Albian age for the

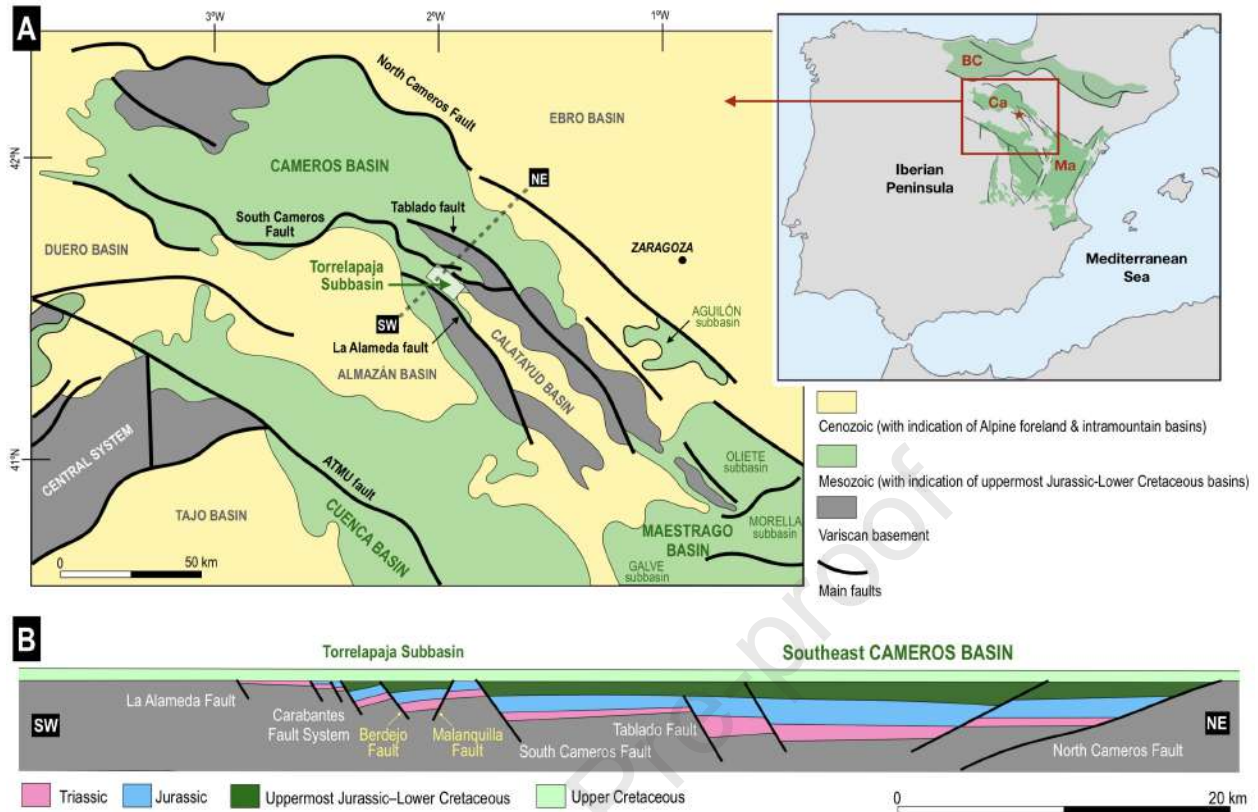
1078 Escucha Fm (see further explanation and discussion in text).

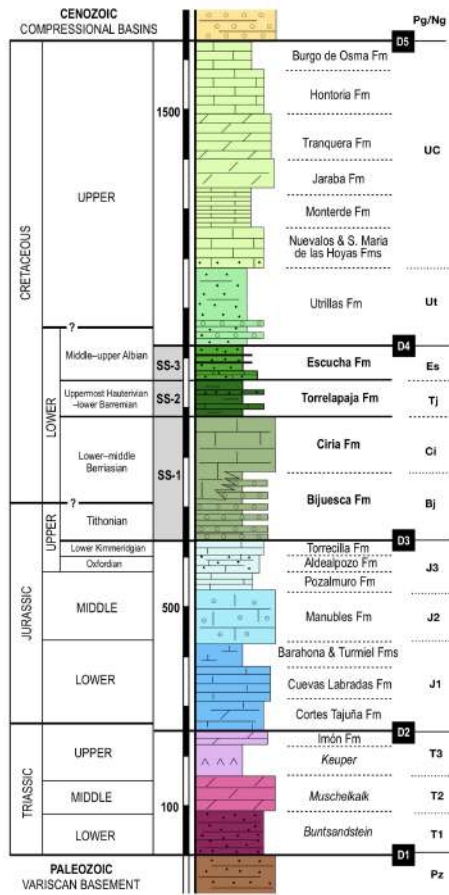
1079 Fig. 14. Proposed equivalence between the synrift sequences recorded in the Torrelapaja Subbasin and
1080 those recorded in the eastern Cameros Basin (mostly based in Clemente, 2010) and the subbasins of the
1081 Western Maestrazgo Basin (compiled from Aurell et al, 2018, 2019b and Liesa et al., 2019; see fig. 1 for
1082 location of basins and subbasins).

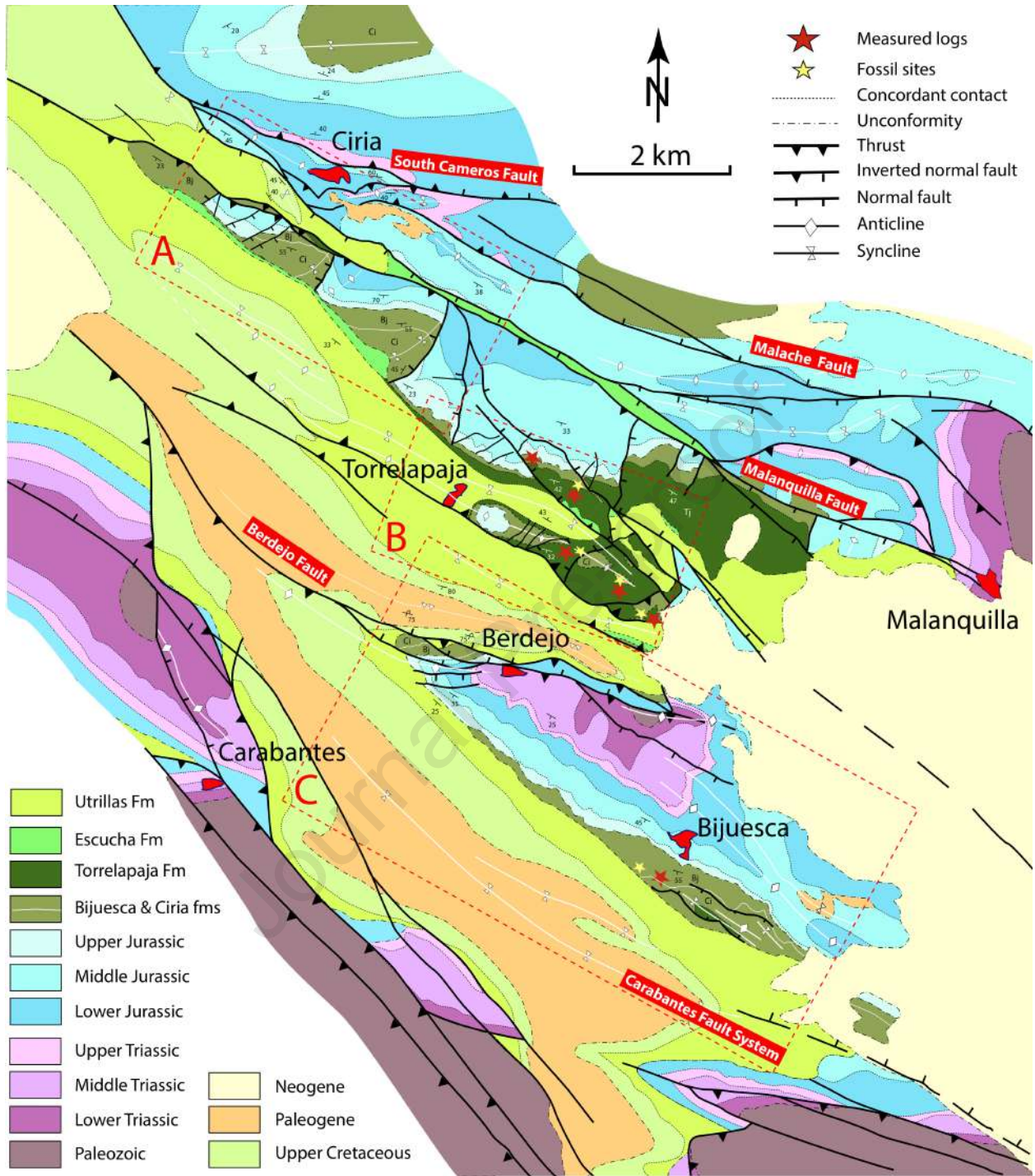
1083 Fig. 15. Idealized geological cross-sections showing the structure of the Torrelapaja Subbasin at the time
1084 of postrift sedimentation (see map for location). 1-1': Transverse view of the Torrelapaja Subbasin
1085 showing the structure of the Bigornia and Bijuesca troughs. 2-2': Longitudinal section along the Bigornia
1086 trough. Note that the NE-SW Cenozoic shortening has not been restored.

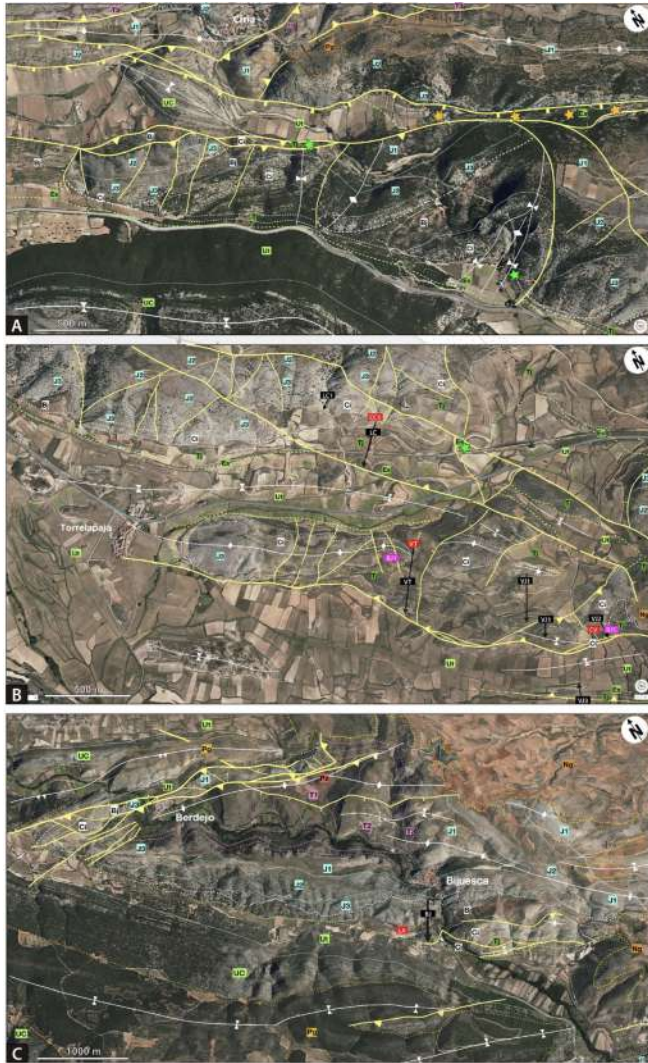
1087 Fig. 16. - Reconstruction of the Bijuesca and Bigornia troughs (Torrelapaja Subbasin) located south of the
1088 South Cameros Fault (inset) during the sedimentation of synrift sequences (SS) 1, 2 and 3 (maps A, B and
1089 C respectively). Specific data of thickness measured in different localities are indicated. Arrows in A and B
1090 indicates palaeocurrent data (the data in SS-1 taken from Sacristán-Horcajada et al., 2012). Note that
1091 maps represent the present-day locations of structures and outcrops, that is without the restoration of
1092 the NE-SW Cenozoic shortening.

1093 Fig. 17. Distribution of main sedimentary domains of Northeast Iberia around (A) the early Berriasian, (B)
1094 the early Barremian and (C) the mid-Albian. Palaeogeography of the Basque-Cantabrian Basin taken from
1095 García (1982), García-Mondejar (1990) and Pujalte et al. (2004). Cameros Basin compiled from Muñoz et
1096 al. (1997), Clemente (2010), Quijada et al. (2013) and Suárez-Gonzalez et al. (2013). Maestrazgo Basin
1097 based on Querol et al. (1992), Aurell et al. (2018, 2019b) and Liesa et al. (2019).



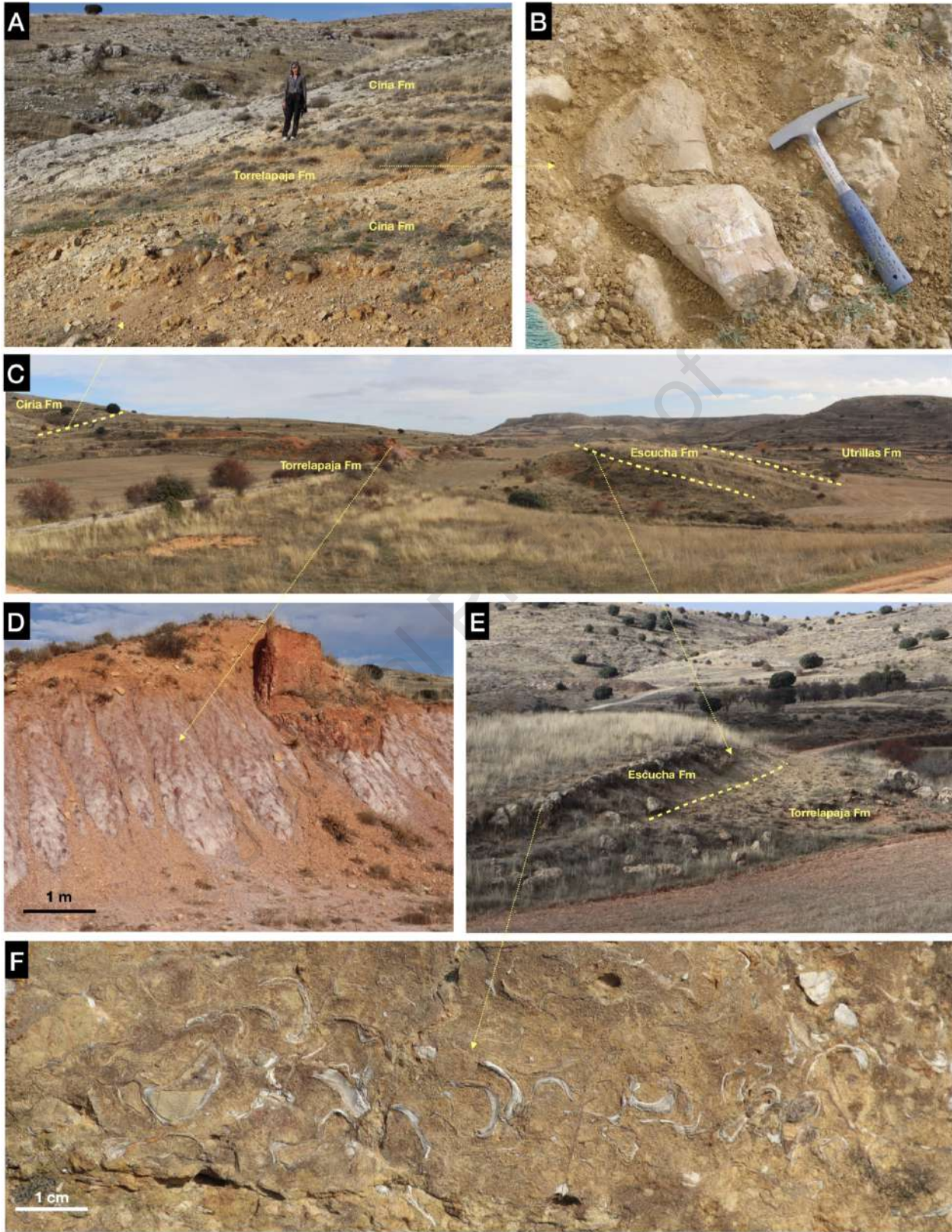


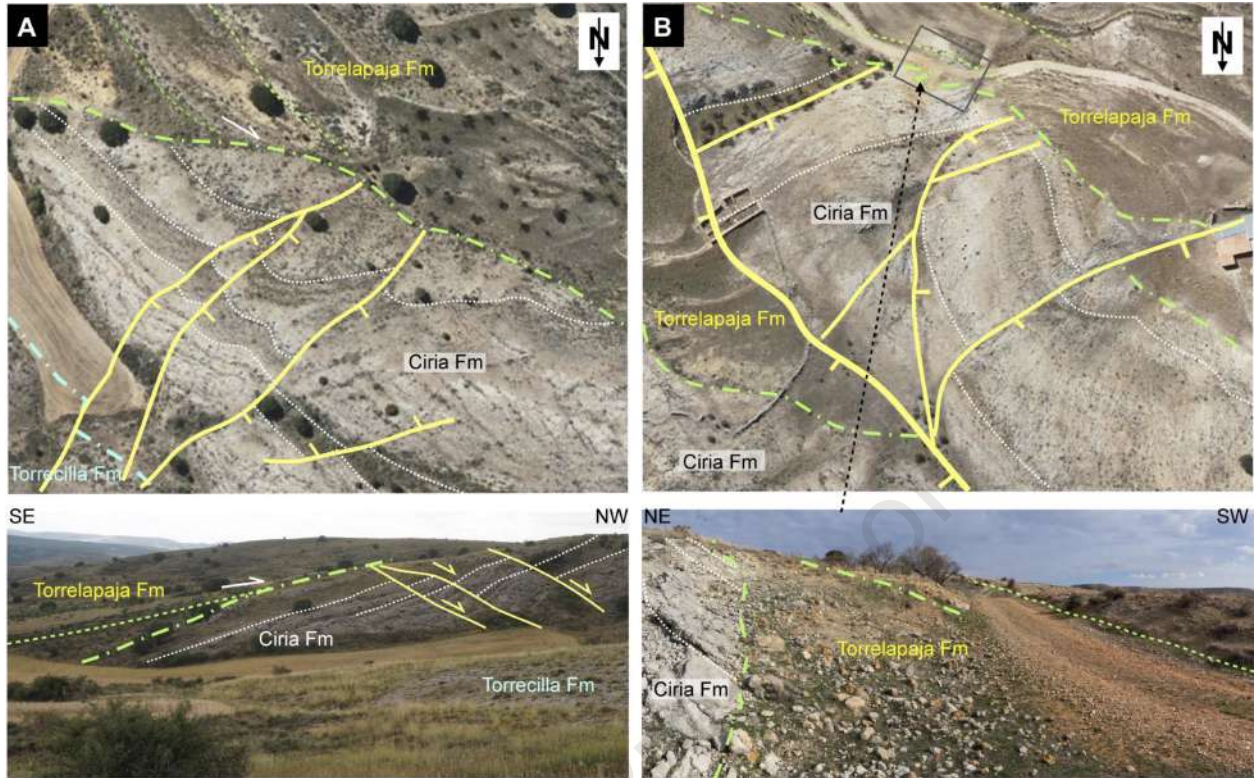


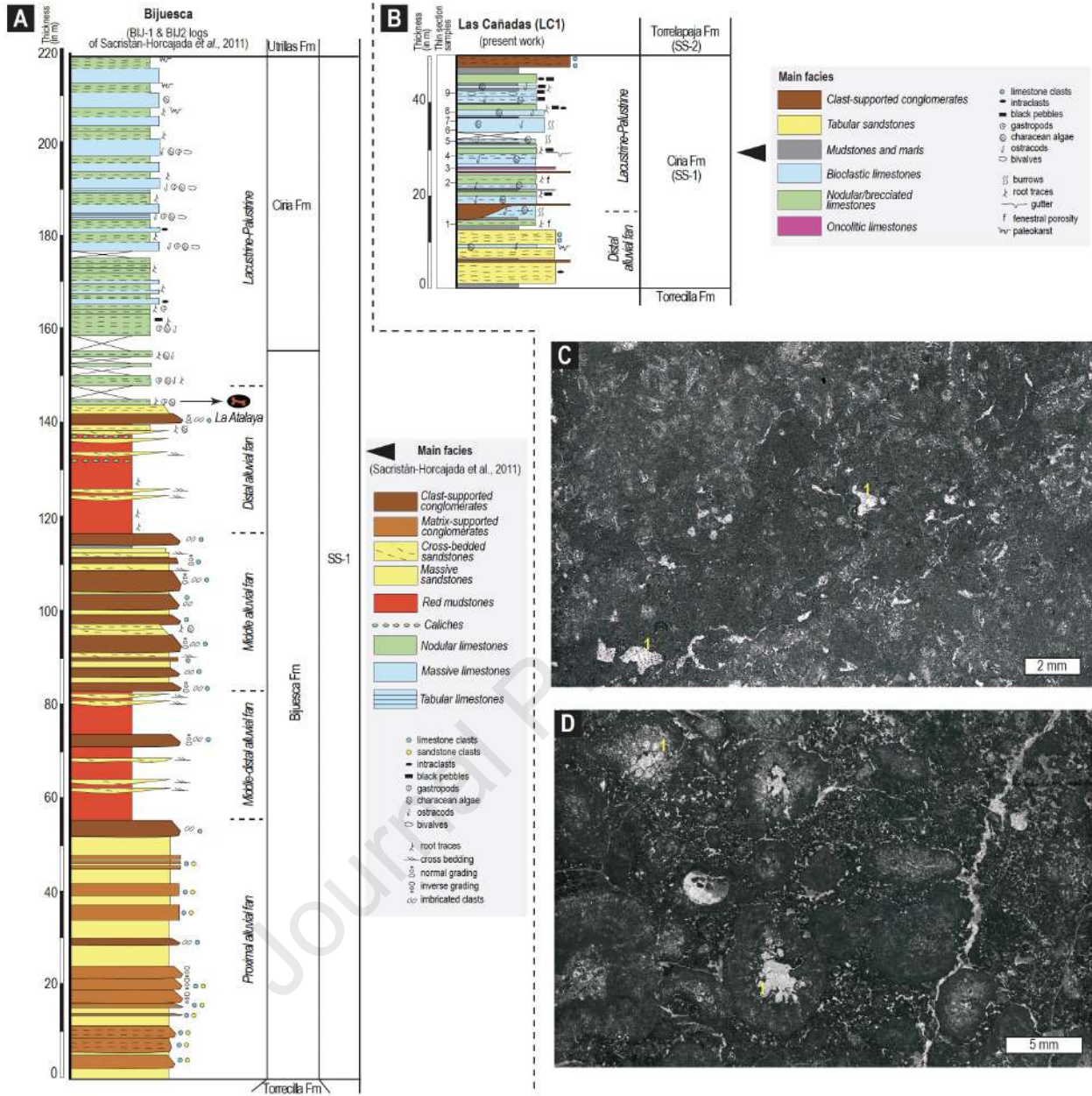


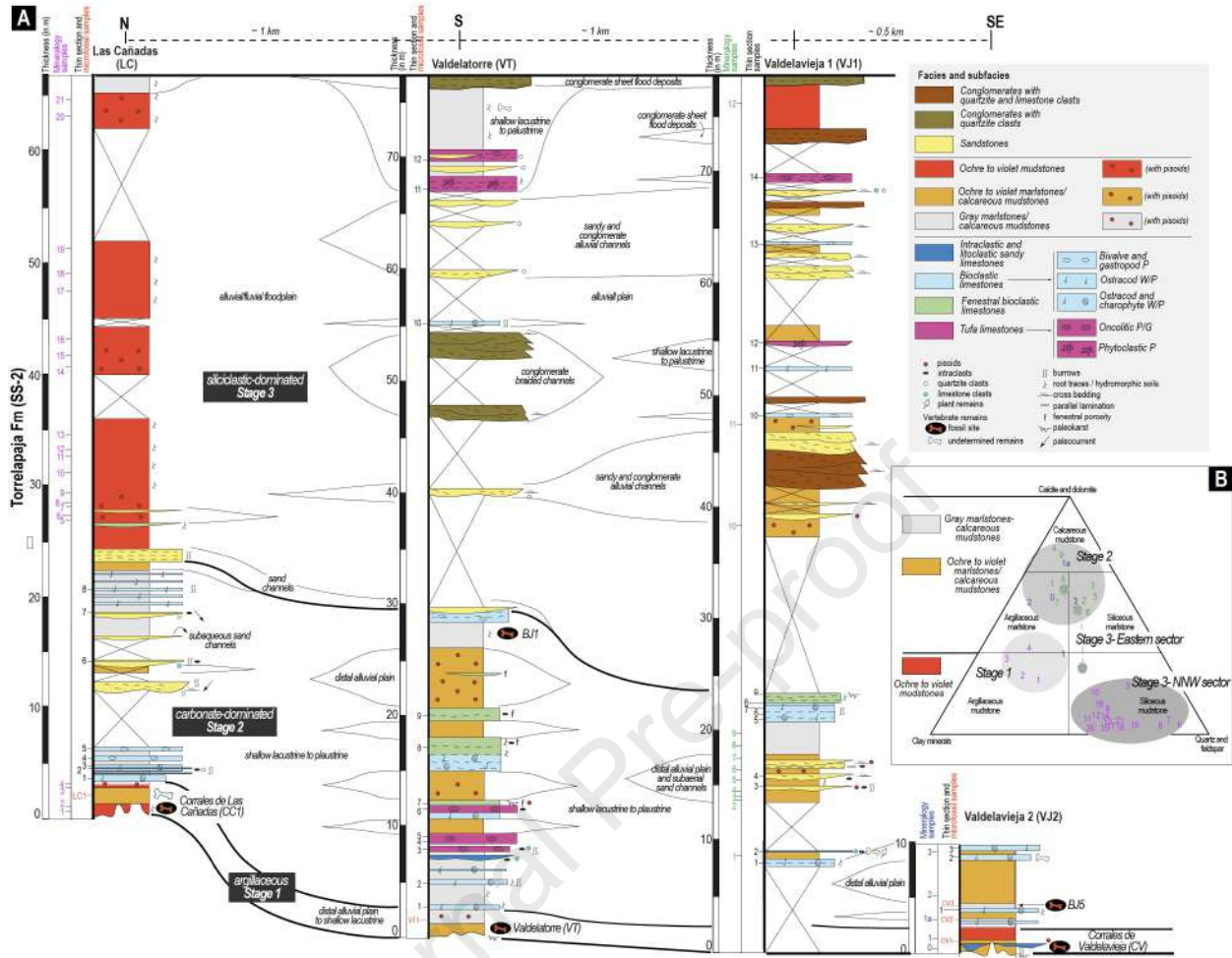


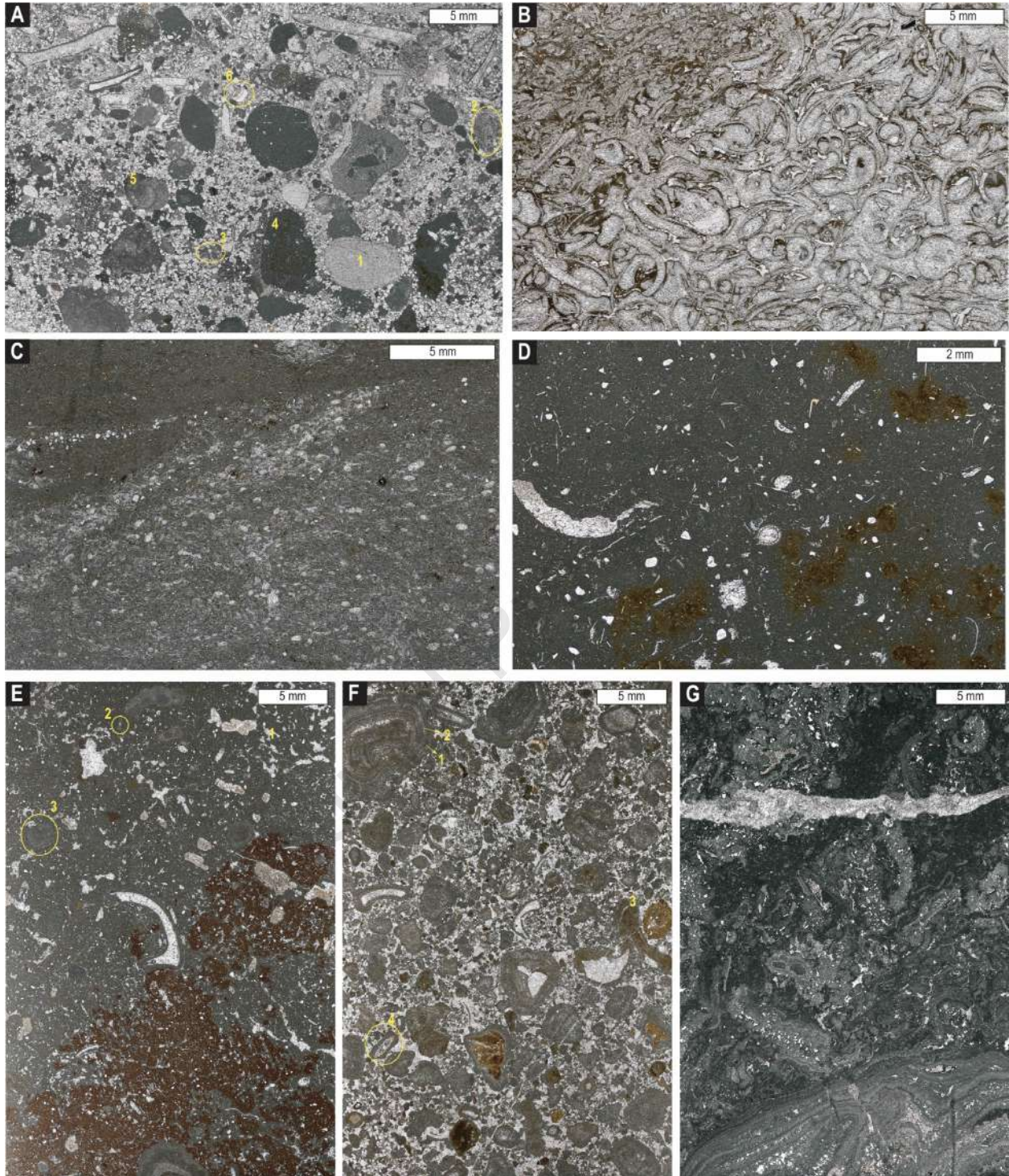


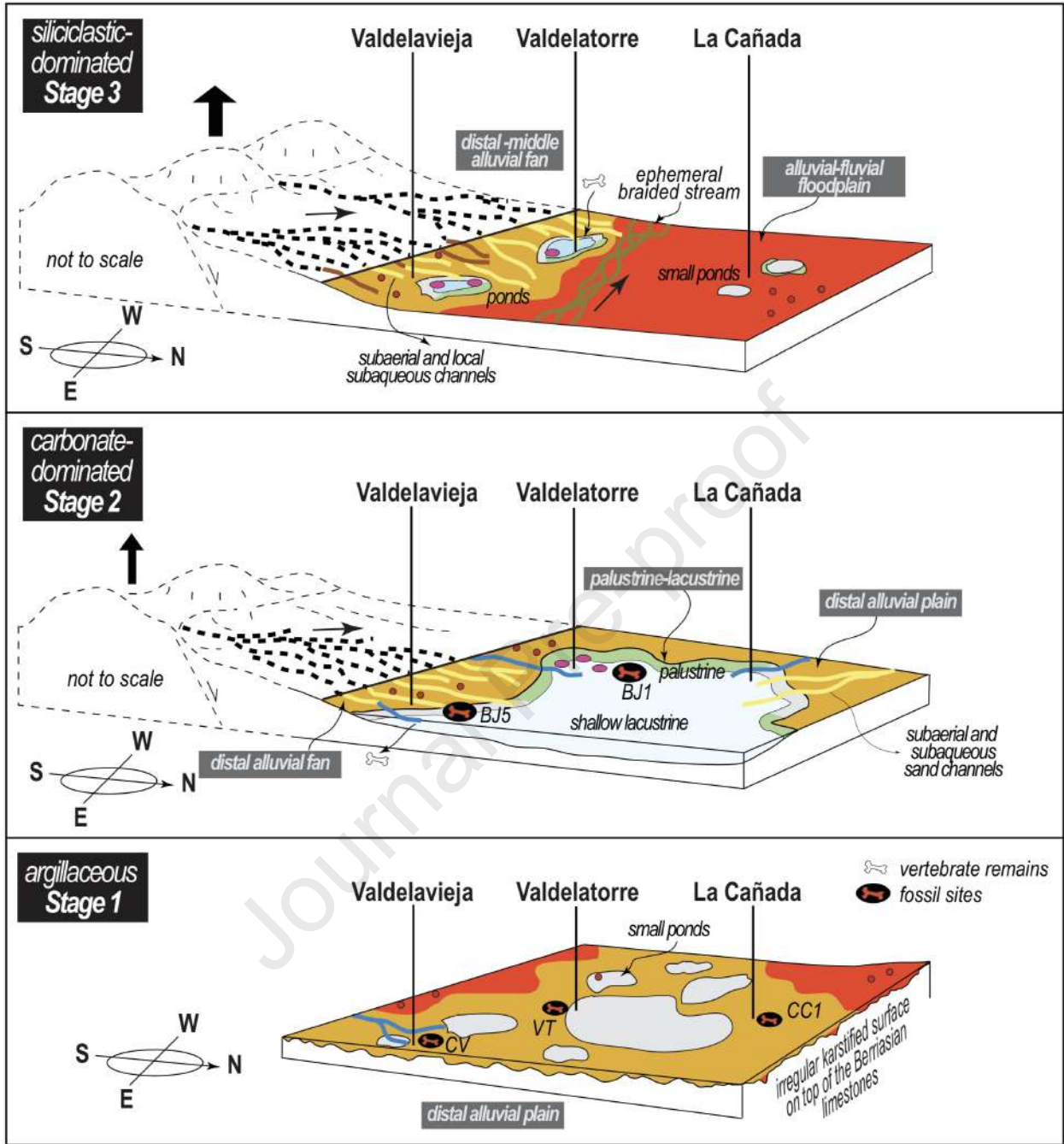


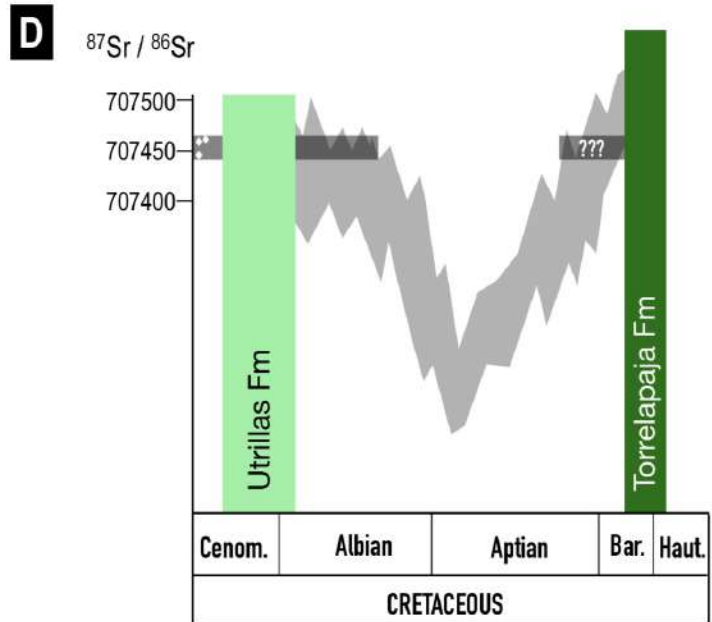
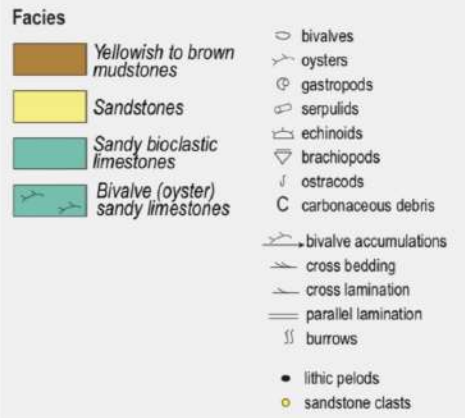
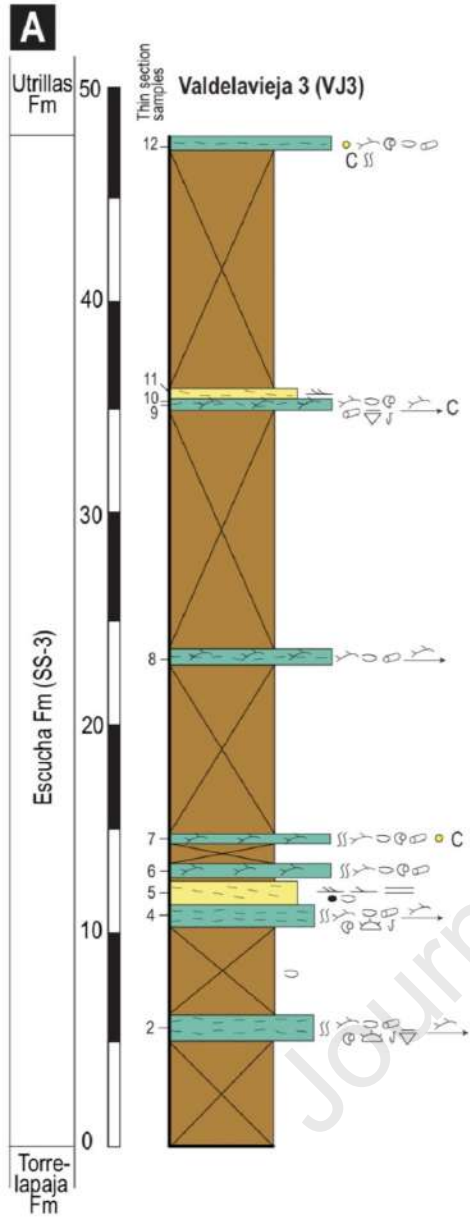








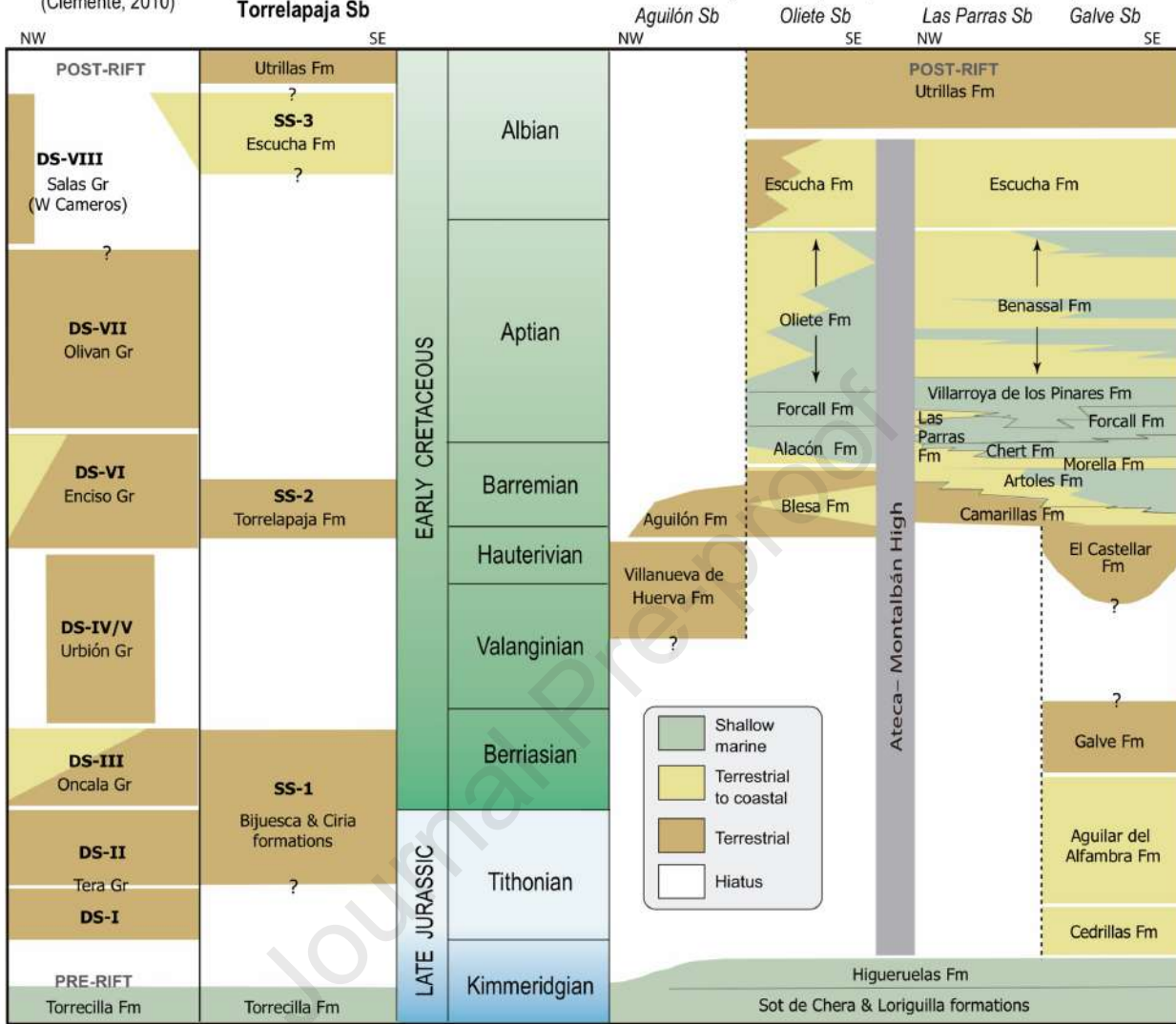


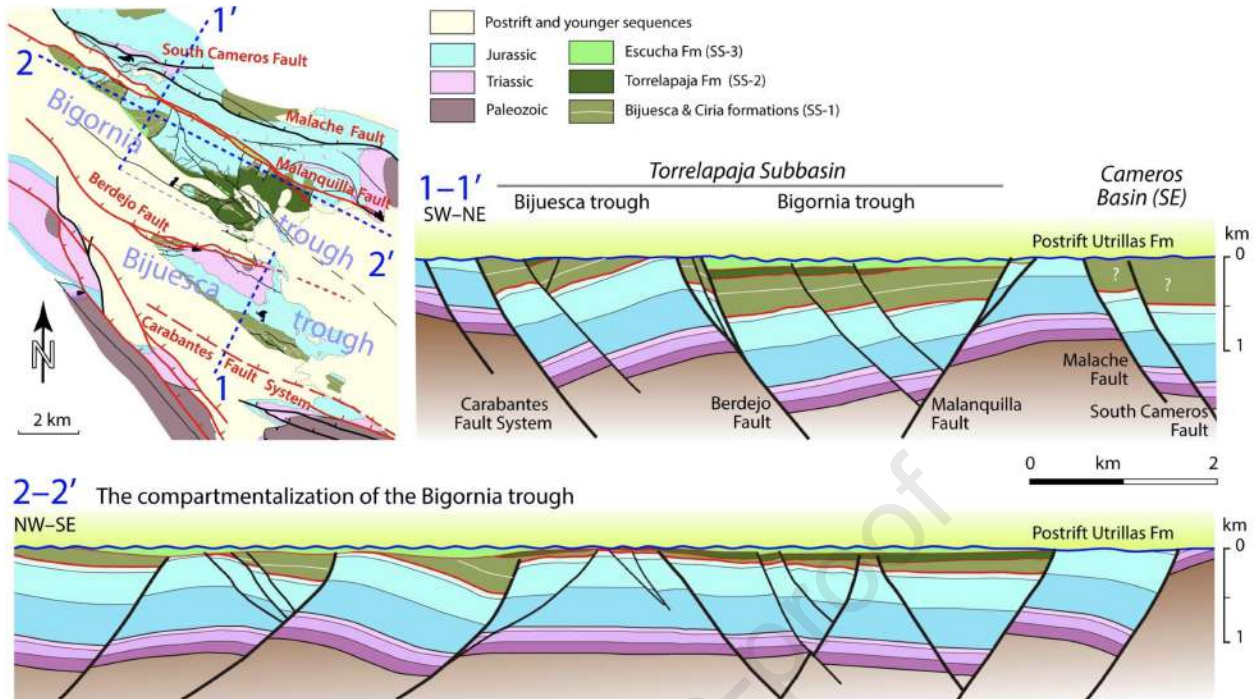


E CAMEROS BASIN
(Clemente, 2010)

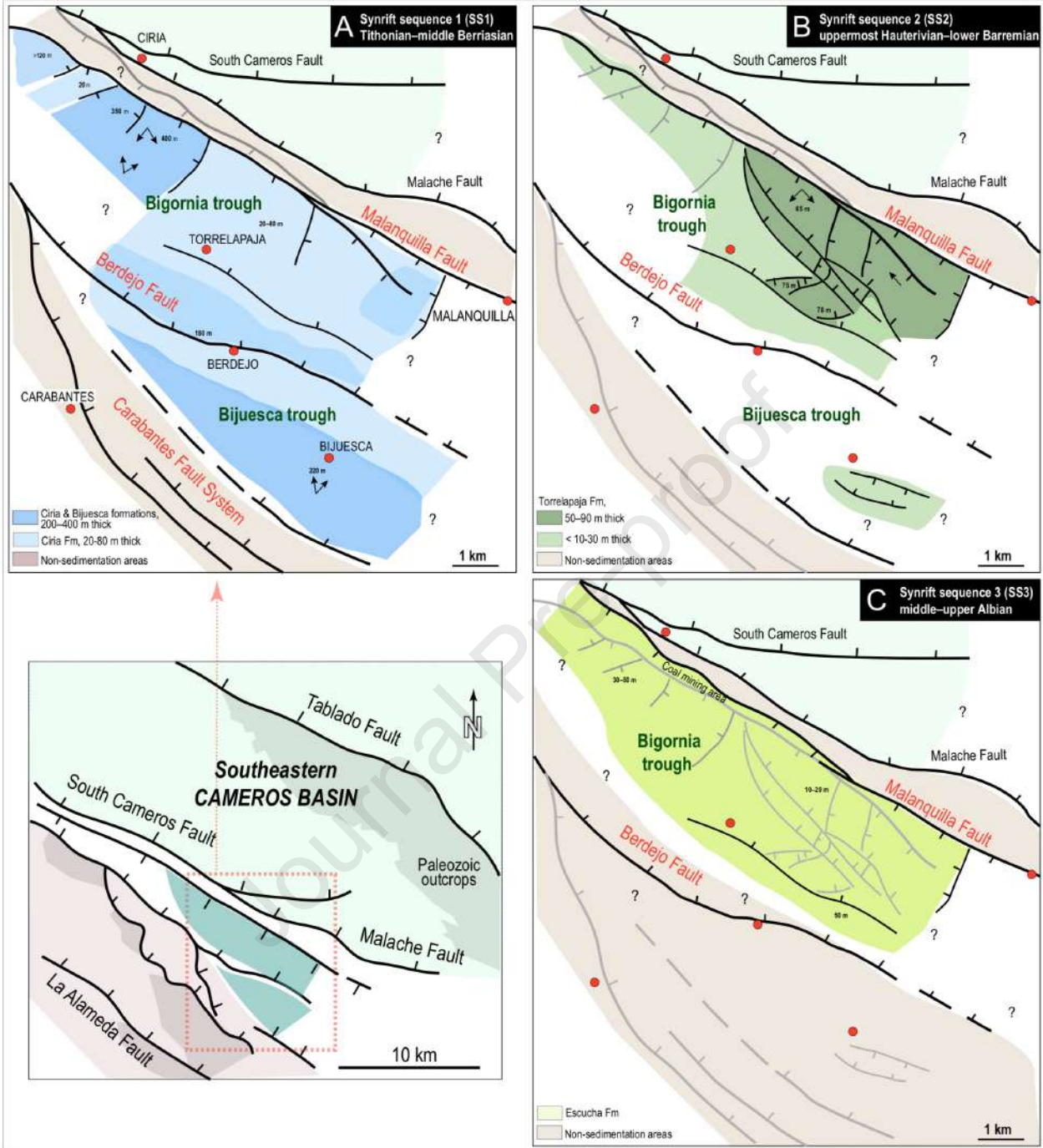
Torrelapaja Sb

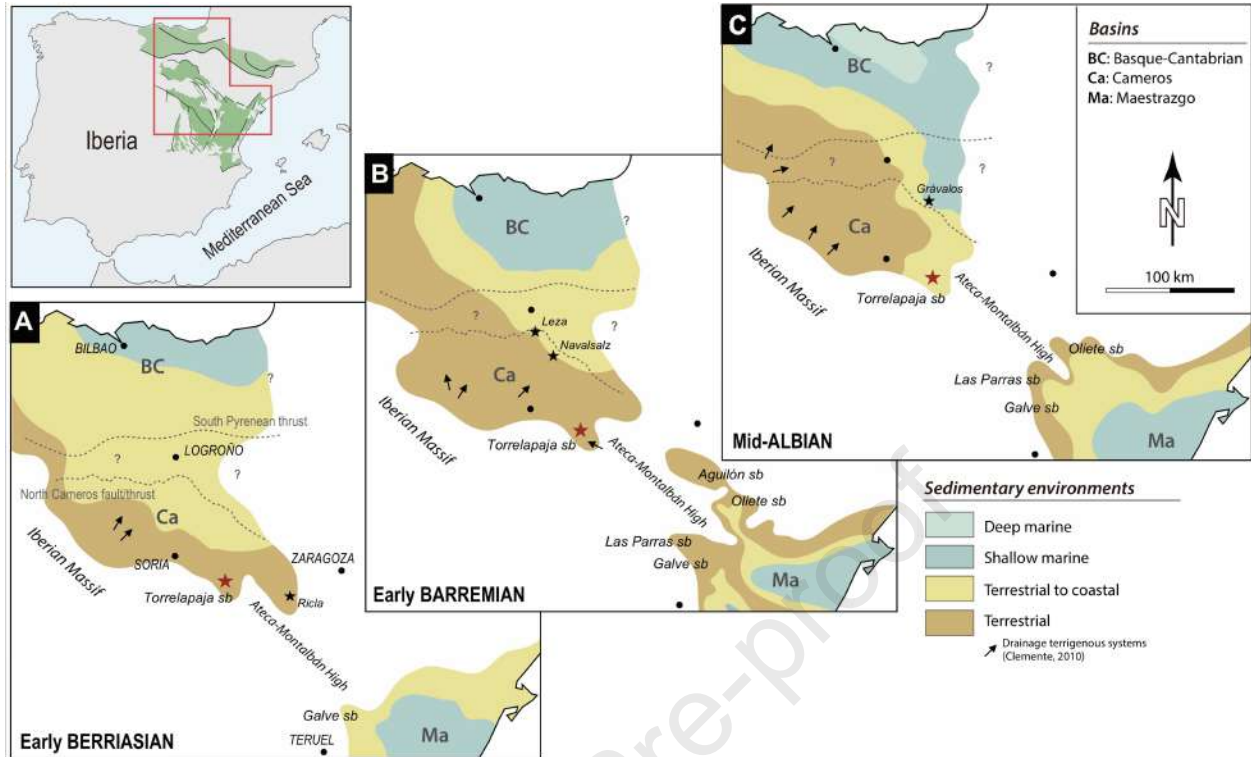
NW and W MAESTRAZGO BASIN
(Aurell et al., 2018, 2019b, Liesa et al., 2019)





Journal Pre-proof





Declaration of interests

The authors declare that they have no known competing financial interests or personal relationships that could have appeared to influence the work reported in this paper.

The authors declare the following financial interests/personal relationships which may be considered as potential competing interests:

Journal Pre-proof